Powerful Forests: The Welfare Implications of Deforestation for the Power Sector*

Rafael Araujo† Francisco Costa ‡ Vinicius Hector §
Marcelo Sant'Anna ¶

First Draft: March 2026; This Draft: March 2026

Abstract

The energy transition depends not only on building renewable capacity but also on protecting the natural resources on which renewables rely. This paper shows that conservation and renewable policies are complements. We quantify how Amazon deforestation affects Brazil's electricity market by reducing rainfall and hydropower generation. We model the transmission chain from deforestation to atmospheric moisture, to downwind rainfall, to river discharge and hydro output, and embed the resulting supply shift within a market-equilibrium framework. Counterfactual simulations indicate that reversing all deforestation since 1985 would increase annual hydroelectric output by 13 TWh, lower electricity prices, and generate welfare gains of USD 1.1 billion per year. These gains are unevenly distributed: consumers benefit from lower prices and Amazon-basin hydropower producers benefit from higher output, while thermal generators and hydropower producers elsewhere lose. Finally, we identify small, high-leverage regions that account for a disproportionate share of hydropower value, informing targeted conservation and restoration.

Keywords: Deforestation, Energy, Amazon, Energy Transition, Renewables.
JEL Codes: Q54, Q23, L94

*We thank Juliano Assunção, Lautaro Chittaro, Eduardo Souza-Rodrigues, and seminar participants at Insper, FGV EPGE, SBE, and Rede PP&S for helpful comments. The authors thank Rede de Pesquisa em Produtividade e Sustentabilidade (Rede PP&S), Amazonia 2030, and Coordenação de Aperfeiçoamento de Pessoal de Nível Superior—Brasil (CAPES)—Grant #001 for the financial support. The funders had no role in the study design, data collection and analysis, interpretation of results, manuscript preparation, or the decision to submit the article for publication.

†FGV EESP Sao Paulo School of Economics. Email: rafael.araujo@fgv.br
‡FGV EPGE Brazilian School of Economics and Finance. Email: francisco.costa@fgv.br
§FGV EPGE Brazilian School of Economics and Finance. Email: vinicius.hector@outlook.com.br
¶FGV EPGE Brazilian School of Economics and Finance. Email: marcelo.santanna@fgv.br

1 Introduction

Natural capital is an input into production in many markets (Costanza et al., 1997; Arrow et al., 2004). When that input becomes scarce, supply shifts, prices move, and rents change hands. In many settings, economic activity determines the supply of natural capital: depletion of aquifers (Bruno and Jessoe, 2021; Ryan and Sudarshan, 2022), species population dynamics (Frank and Oremus, 2025), clean air (Currie and Walker, 2019), and climate stability (Nordhaus, 2019). With sufficient depletion, natural capital may even collapse (Brander and Taylor, 1998). When natural capital connects multiple economic activities, depletion in one sector can shift market fundamentals in others. While prices adjust economy-wide, welfare effects depend on agents' heterogeneous exposure to the affected resource.

This paper shows how land use affects electricity markets through its impact on rainfall and hydropower generation. The global energy transition requires large expansions in renewable generation. Many emerging economies rely heavily on hydropower, a low-carbon electricity source (Gernaat et al., 2017). At the same time, these countries face intense pressure to convert forests and other natural lands for agriculture and resource extraction (Balboni et al., 2023). Policy debates often treat conservation and the energy transition as separate objectives. We highlight a neglected complementarity: forests sustain rainfall that raises hydropower supply, so conservation policy becomes a supply-side policy for clean electricity.

We study this complementarity in Brazil. The country contains the majority of the Amazon rainforest—the world's largest tropical forest and a dominant driver of continental moisture transport—while deriving most of its electricity from hydropower. We model the complete transmission chain from deforestation to welfare: forest loss reduces atmospheric moisture and lowers rainfall in catchment areas, decreasing river discharge and clean electricity generation. This forces greater reliance on higher-cost thermal generation, shifting supply and changing equilibrium prices and quantities. This framework yields a market-based valuation of forest ecosystem services—complementary to carbon-focused approaches—and traces welfare effects across consumers and heterogeneous producers.

Our empirical approach has two parts. First, we estimate how deforestation shifts hydropower supply by linking forest cover to rainfall, river discharge, and electricity generation. We begin by estimating the causal effect of upwind forest cover on rainfall, building on the atmospheric moisture–recycling framework (Spracklen et al., 2012;

Araujo, 2023). Identification arises from year-to-year variation in high-altitude atmospheric circulation that alters which forests lie upwind of a given location, while holding local characteristics and aggregate shocks fixed. We then map rainfall into river discharge at each hydropower plant using a parsimonious log-log relationship between cumulative upstream precipitation and flow, consistent with standard hydrological models. Finally, we convert discharge into electricity generation using the physical relationship between water flow and energy output. Combining these steps, we compute the implied change in hydropower supply under counterfactual forest-cover scenarios.

Second, we translate these supply shifts into equilibrium and welfare effects. We construct an empirical supply curve from plant-level operating cost data and merit-order dispatch rules. This model determines equilibrium prices and quantities for alternative reforestation scenarios while capturing heterogeneous producer impacts. Hydropower plants experience ambiguous welfare changes—lower prices but higher dispatch—with heterogeneity driven by varying upwind forest exposure, while thermal generators unambiguously lose from decreased dispatch and lower prices.

Our counterfactual simulations indicate that reversing all deforestation since 1985 (about 840,000 km^2) would increase annual hydroelectric output by 13 TWh, roughly 2% of Brazil's current electricity consumption. This outward shift in low-cost supply reduces reliance on thermal generation and lowers the equilibrium electricity price by about 2%, generating welfare gains of USD 1.1 billion per year. This aggregate gain masks substantial redistribution across market participants. Consumers gain USD 916 million annually from lower prices. Producer effects are heterogeneous. Hydroelectric plants in the Amazon basin gain USD 543 million from higher output, while plants in other basins lose USD 235 million as the drop in prices outweighs the production gains. Thermal generators lose USD 129 million due to lower dispatch and lower prices. Reduced thermal generation also lowers carbon emissions, yielding social benefits valued at USD 175 million per year.

Finally, we show that the forest's contribution to energy security is highly uneven across space. Atmospheric circulation determines where forest moisture travels, while river networks determine where rainfall translates into hydropower generation. As a result, a small share of the Amazon accounts for a disproportionate share of hydropower-relevant rainfall. Using our estimated mapping, we rank forest pixels by their contribution to hydropower output and show that targeted conservation or restoration in energy-relevant areas can deliver a large share of the sector's welfare gains. We find that just 3.3% of the Amazon accounts for 20% of its total value for hydropower. These

high-value areas overlap substantially with the 'Arc of Deforestation,' implying that the locations under the most pressure from agricultural expansion are also those with the highest value for electricity markets.

This paper contributes to three strands of the literature. First, it relates to a growing body of work on how environmental constraints affect market equilibrium outcomes. Recent research quantifies how scarcity of natural inputs such as water alters production, trade, and welfare, and how institutions governing allocation shape these effects (Costinot et al., 2016; Ryan and Sudarshan, 2022; Ferguson, 2024). Our framework applies broadly to settings in which ecosystem services shift market supply curves and natural resource constraints shape market equilibrium. In our setting, the relevant natural capital is endogenous to economic activity elsewhere and affects markets through ecosystem services rather than direct extraction. As a result, those who cause the degradation differ from those who bear its costs. This environmental feedback implies that infrastructure planning that treats environmental conditions as fixed can misstate the returns to investments in climate-sensitive sectors (Hsiao, 2023; Balboni, 2025), including renewable generation. Moreover, the externality generates heterogeneous and potentially ambiguous welfare effects through the product market equilibrium. Resource depletion raises equilibrium prices of final products, benefiting producers with limited exposure to the shortfall even as it harms those most affected. This heterogeneity can shape incentives to finance conservation or restoration efforts.

Second, we contribute to the valuation of ecosystem services and forests (Ferraro et al., 2012). The dominant approach values forests through avoided carbon emissions, but social cost of carbon estimates vary by an order of magnitude and remain contested (Tol, 2023). We provide a complementary market-mediated valuation channel that prices non-market ecosystem services by their effects on electricity markets. While existing studies link forest cover to hydrological and hydropower outcomes (Stickler et al., 2013; Araujo, 2024), they do not embed these physical relationships in the electricity-market equilibrium. By doing so, we quantify price effects and trace welfare incidence across consumers and heterogeneous producers. We also contribute to the literature on the consequences of deforestation (Balboni et al., 2023; Costa et al., 2025). Much of this work treats climate as exogenous to land-use decisions, missing feedback from deforestation to local climate (Souza-Rodrigues, 2019; Domínguez-Iino, 2026; Assunção et al., 2023; Farrokhi et al., 2025; Araujo et al., 2026). Exceptions include Araujo (2023) and Grosset et al. (2023) for agriculture. Our electricity-sector channel adds another dimension to this feedback, broadening the cost-benefit analysis

of forest conservation and restoration policy.

Third, we contribute to the literature on the energy transition and electricity markets (Borenstein and Kellogg, 2023; Gonzales et al., 2023; Besley and Persson, 2023; Gowrisankaran et al., 2024; Ito, 2025; Fabra and Llobet, 2025; Butters et al., 2025; Hausman, 2025; Jha and Leslie, 2025). This literature examines the integration of renewable generation into electricity markets, the role of storage, transmission, and how policy can deliver decarbonization. We highlight a complementary margin: the effective supply of renewable electricity may depend on environmental conservation. Degrading natural capital can reduce the output and returns of existing clean energy infrastructure. Our results imply that conservation can raise the returns to clean electricity and strengthen decarbonization: energy policy and land-use policy are complements in hydropower-dependent systems.

The remainder of the paper is organized as follows. Section 2 describes how forests affect rainfall and outlines the Brazilian power sector. Section 3 presents the data. Section 4 develops the empirical framework linking deforestation to hydropower generation. Section 5 presents the conceptual framework for equilibrium and welfare analysis in electricity markets, and Section 6 connects the model to the data. Section 7 presents the main results and welfare analysis. Section 8 concludes.

2 Background

This section provides background on the role of the Amazon rainforest in Brazil's climate and on the institutional structure of the Brazilian power market.

Flying Rivers. The Amazon is central to Brazil's climate. The continental hydrological cycle begins over the ocean where the Sun's energy evaporates ocean water, atmospheric transport then carries the moisture inland, and precipitation follows. In the presence of tropical forests, a recycling mechanism increases the level and extends this transport of moisture: precipitation is absorbed by trees and returned to the atmosphere through evapotranspiration, sustaining the moisture flux. The Amazon rainforest performs this function at continental scale, releasing large volumes of water vapor that carry moisture thousands of kilometers beyond the forest (Salati et al., 1979; Wunderling et al., 2022). This process consists of the "flying rivers" of the Amazon (Marengo et al., 2018).

Deforestation, however, weakens this mechanism. Fewer trees add less water vapor

to the atmosphere, leading to persistent rainfall declines across Brazil (Spracklen et al., 2012; Smith et al., 2023). This climatic externality can have major economic effects, through farming (Araujo, 2023), river transport, and energy supply. We focus on the last. Brazil relies heavily on hydropower, with more than half of its electricity coming from hydro plants in 2023.[1] Less rainfall means less water to spin turbines, constraining generation.

The Brazilian Power Market. Brazil operates a centralized dispatch system. The National System Operator (ONS) decides which power plants to activate and controls their production levels. The ONS directly operates all plants above 30 MW of installed capacity, which account for 83% of Brazil's total installed capacity.[2] Each week, thermal plants report their variable operating costs per megawatt-hour. The ONS ranks plants from lowest to highest cost and dispatches them accordingly. Low-cost sources—hydro, wind, solar, and nuclear—are prioritized over expensive thermal plants. This merit-order system determines which plants operate at any given time, with cheaper plants running first and more expensive plants activated when demand rises or hydro availability declines.

Renewables dominate the Brazilian electricity mix.[3] In 2023, they supplied 81% of generation: 60% hydro, 14% wind, and 7% solar. This makes Brazil the G20's cleanest power producer (Ember, 2025). In comparison, these sources provide 39% of generation in the EU, 29% in China, and 21% in the United States. Thermal plants supply the rest of Brazil's electricity. These include nuclear, gas, coal, biomass, and diesel plants. Thermal plants are usually the most expensive and serve as marginal suppliers, operating when renewable generation falls short.

3 Data

We model the effect of deforestation on the Brazilian power market by integrating multiple datasets on the geometry of hydrographic basins, Amazon forest cover, atmospheric trajectories, rainfall, hydropower plants, river discharge, electricity generation, and operating costs.

[1] Hydropower's share in Brazil's electricity mix was higher in the past, peaking at 84% in 2009.

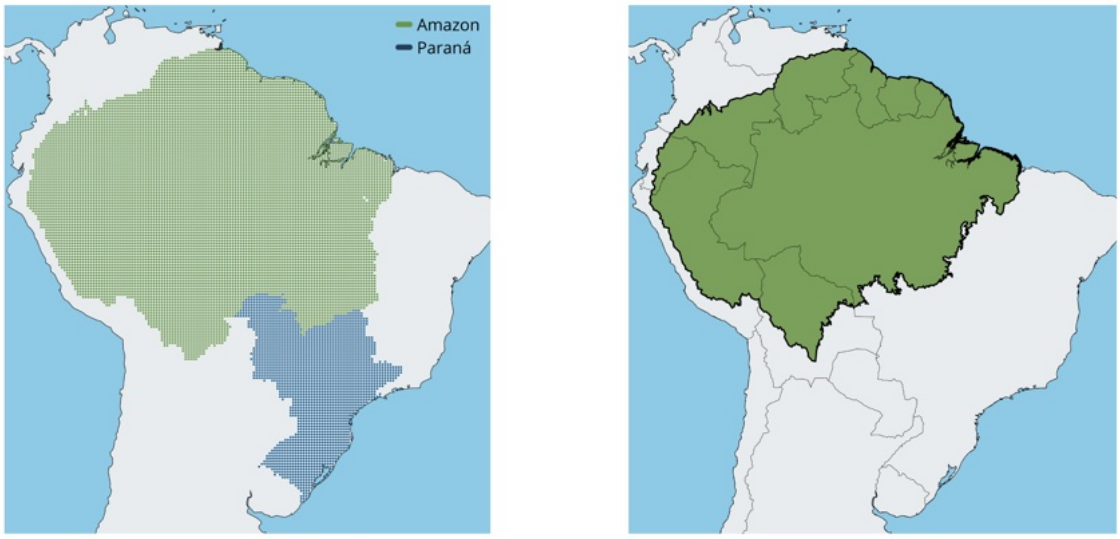
[2] Smaller plants either coordinate partially with the ONS or inject power independently without centralized dispatch (Operador Nacional do Sistema Elétrico (ONS), 2025d).

[3] Renewables include hydro, solar, wind, and biomass power plants.

Hydrographic Basins. WWF's HydroBASINS (Lehner and Grill, 2013) provides the geometries of hydrographic basins across South America. A basin is the land area where all water, including rivers and rainfall, flows to a single point. This is primarily defined by topography. We focus on the Amazon and Paraná river basins, as those are affected by the Amazon moisture flows.[4] We then overlay a 0.25° grid on this area, which serves as our main spatial units of observation (Figure 1a).

Amazon Forest Cover. MapBiomas (2025) provides annual land use and land cover data for the Amazon at 30 m resolution from 1985 to 2020 (Figure 1b displays the Amazon region). We aggregate these data to 0.25° × 0.25° pixels and compute the fraction of each pixel covered by forest, with values ranging from 0 (completely deforested or outside the Amazon biome) to 1 (fully forested). We then overlay these measures on the original grid to track the evolution of forest cover across time and space.[5]

Figure 1: The Amazon Rainforest and the Main Grid



(a) Main Grid (b) The Amazon Rainforest

Notes: Figure (a) shows the grid with the pixels we use in our analysis. Those pixels are split by basin: Amazon and Paraná as of Lehner and Grill (2013). Figure (b) shows the area of the Amazon.

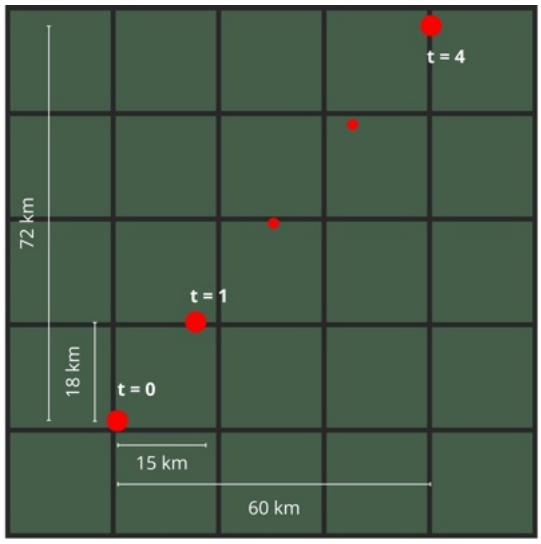
[4]We crop the Paraná basin to its Brazilian portion, which is the only portion that feeds Brazilian hydropower plants. For the Amazon basin, we include portions in other countries, since these regions also feed Brazilian hydropower plants.

[5]We restrict the definition of forest to natural tropical forest cover within the Amazon biome, following the borders set by Eva et al. (2005).

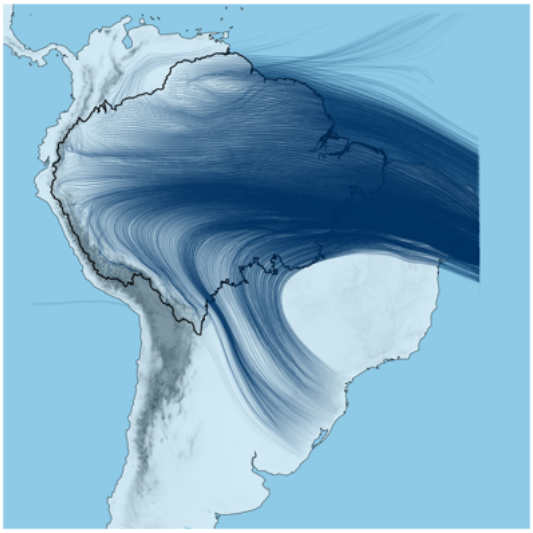
Atmospheric Trajectories ECMWF's ERA5 (Copernicus Climate Change Service (C3S), 2017) provides the average monthly wind speed components (longitudinal (U), latitudinal (V), and vertical (W)) for each grid cell from 1985 to 2020. The original data consist of monthly rasters with the mean U, V, and W wind speed components for every 0.25° pixel in South America. Since we know the wind speeds for each air parcel, we can work backward and find where the parcel was one hour earlier, then two hours earlier, and so on. We repeat this process for up to 168 hours (7 days), which is sufficient for most air parcels to traverse the entirety of South America.

We apply this algorithm to each pixel in the Amazon and Paraná basins, identifying all upwind source pixels for each month-year. Each pixel i thus has one back-trajectory per month-year tracing the atmospheric path that brings moisture to that pixel. Figure 2 illustrates the construction method and displays actual trajectories for a representative month.

Figure 2: Examples of Back Trajectories



(a) Construction Example



(b) Real Set of Back Trajectories

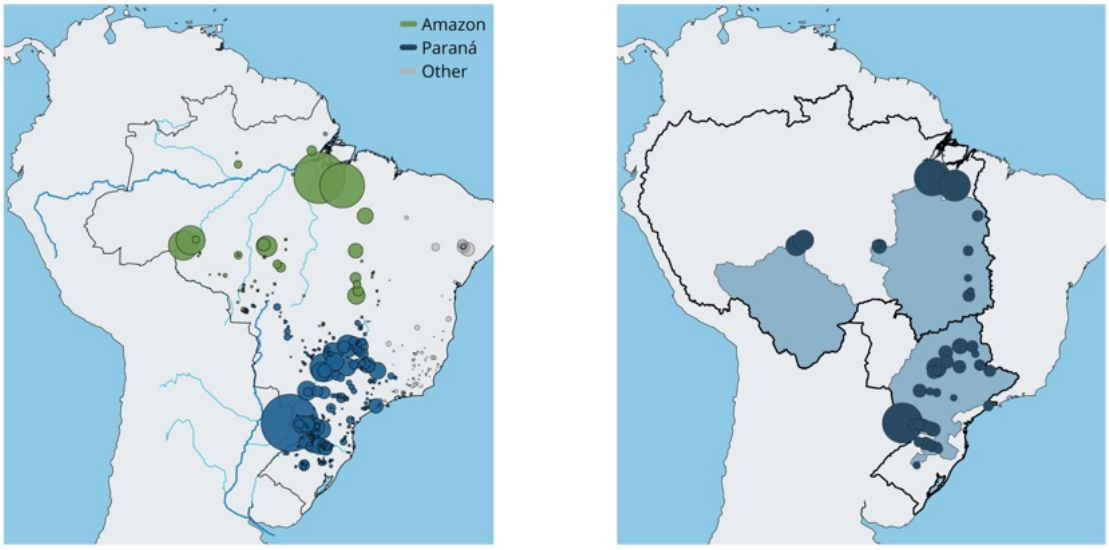
Notes: Figure (a) shows a simplified example of how we construct each back-trajectory. Suppose the wind in all pixels has an east–west (U) constant speed of 4 m/s and a south–north (V) constant speed of 4.15 m/s. The analysis begins at $\tau = 0$. One hour earlier ($\tau = 1$), the air parcel would be 15 km farther east and 18 km farther north. Four hours earlier, it would be 60 km east and 72 km north. We extend this calculation up to 168 hours into the past. Figure (b) shows the set of observed back-trajectories in September 2015 that cross the Amazon Rainforest. Air parcels originate over the Atlantic Ocean, move across the forest, and reach regions as far south as southern Brazil. Wind speeds and directions vary across time and space.

Rainfall. ECMWF's ERA5 (Copernicus Climate Change Service (C3S), 2017) also provides the daily mean precipitation for each month for each point. We aggregate the data to annual precipitation for each pixel between 1985 and 2020.

Hydropower Plant Locations. The Brazilian electricity system operator (Operador Nacional do Sistema Elétrico (ONS), 2025a) informs locations and installed capacities (in MW) for all large plants. This includes all hydro, thermal, large solar, wind, nuclear, and biomass stations, and excludes decentralized solar. Figure 3a shows the country's hydropower plants per basin.

Upstream Catchment Areas. The HydroBASINS dataset (Lehner and Grill, 2013) partitions drainage basins into hierarchically indexed sub-basins and identifies upstream-downstream relationships. For each sub-basin, it provides the upstream catchment area—the land area from which all water reaching that basin originates—following the method proposed by Pfafstetter (1989). We use these data to delineate the catchment area for each hydropower plant (Figure 3b).

Figure 3: Hydropower Plants in Brazil and Their Catchment Areas



(a) Hydropower Plants Locations

(b) Main Catchment Areas

Notes: Figure (a) shows where the main hydropower plants are in Brazil, while Figure (b) shows the main catchment areas, whose power plants account for nearly 90% of the hydroelectric output in the Amazon and Paraná Basins.

River Discharge. Operador Nacional do Sistema Elétrico (ONS) (2025c) reports daily mean river discharge for all centrally dispatched hydropower plants with installed capacity above 30 MW.[6] We aggregate daily data to annual means (2000 to 2024) to capture long-run hydrological conditions relevant to power generation.

Energy Generation. Operador Nacional do Sistema Elétrico (ONS) (2025d) provides hourly electricity output (in MWh) for each plant. We aggregate these observations (2000 to 2024) to obtain the total annual generation per plant-year.

Thermal Power Plants Operating Costs. Thermal power plants report their weekly operating costs per unit of MWh produced (Operador Nacional do Sistema Elétrico (ONS), 2025b). This is influenced by factors such as the price of fuel, payroll, and maintenance costs. We use average operating costs from 2021 to 2024 per power plant to build the aggregate supply curve in Section 6.

4 Deforestation on Hydropower Energy: Empirical Model

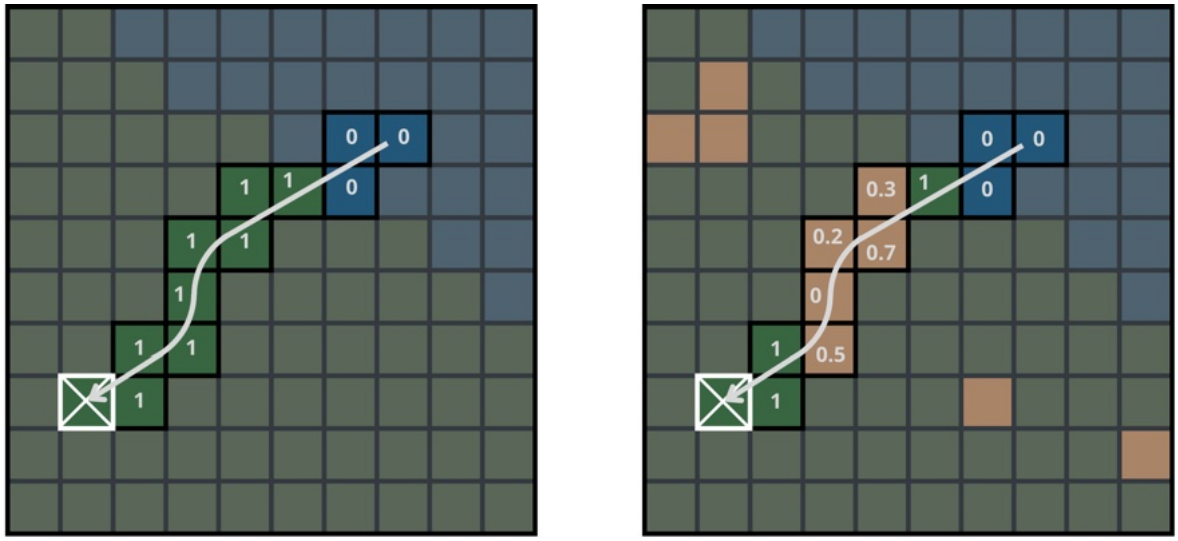
To model the impact of deforestation on hydropower generation, we decompose it into three separate components. We begin by measuring the impact of deforestation on rainfall through a causal model. Then, we use a predictive model to convert rainfall into river flow, which serves as the main input into the hydropower production function. Finally, we map river flow on energy generation using a production function from physics.

Deforestation on Rainfall. The model connecting deforestation and rainfall follows Araujo (2023). Each forested pixel in the Amazon increases atmospheric humidity through evapotranspiration and the recycling of rainfall water, as discussed in Section 2. This humidity is transported downwind by atmospheric circulation, affecting rainfall hundreds or even thousands of kilometers away. To measure the impact of the forest on rainfall, we need two variables: rainfall in pixel i and the exposure of pixel i to upwind forest, which we call "upwind forest." The rainfall variable is available directly as data, but the upwind forest variable must be constructed.

[6] Smaller, decentralized plants account for roughly 10% of Brazil's installed hydropower capacity but are not centrally dispatched and are excluded from this dataset.

We model atmospheric circulation to trace the humidity that passes over the Amazon before reaching each pixel. This approach follows Araujo et al. (2023) and Spracklen et al. (2012). We overlay atmospheric trajectories with forest cover to construct a measure of upwind forest for each year-month-pixel. Figure 4 illustrates this step. In the example, the trajectory starts in the ocean and ends just before the reference pixel. In panel (a), the backward trajectory passes over $(8 \times 1) + (3 \times 0) = 8$ forested pixels. In panel (b), it passes over $(3 \times 0) + (0.3 + 0.7 + 0.2 + 0 + 0.5) + (3 \times 1) = 4.7$ forested pixels.

Figure 4: Example of a Trajectory Under Two Forest Cover Scenarios



(a) No Deforestation

(b) Partial Deforestation

Notes: This figure illustrates how we compute the upwind forest cover measure for a single reference pixel i, shown in white. Pixels over the ocean and outside the Amazon are assigned zero forest cover. Forest pixels outside the upwind trajectory do not affect the upwind forest exposure of i. Figure (a) shows a trajectory with no deforestation, while Figure (b) shows the same trajectory with partial deforestation. For simplicity, this example abstracts from distance weights, which are applied in the analysis in Section 7.

For each reference location i, let B_{imt} denote the set of upwind pixels along its back-trajectory in month m of year t. More distant pixels contribute less to downwind rainfall, and we measure distance as the travel time in hours from pixel j to reference pixel i, denoted by $s_{mt}(i, j)$. Let p_{jt} denote the share of forest cover in pixel j, we then

measure upwind forest cover as:

$$f_{it} = \sum_{m} \sum_{j \in B_{imt}} \theta^{s_{mt}(i,j)} p_{jt},$$

where $0 < \theta < 1$ is a parameter that discounts distance.[7] Upwind forest is thus a distance-weighted sum of upwind forest cover. A larger f_{it} means more forest upwind of location i. A larger θ increases the influence of distant forest on the reference pixel i rainfall. The climate model linking forest cover to rainfall is given by:

$$r_{it} = \alpha_i + \alpha_t + \beta f_{it} + \varepsilon_{it}, \tag{1}$$

where r_{it} is rainfall at pixel i in year t, and α_i and α_t are pixel and year fixed effects. The parameter β captures the causal effect of deforestation or reforestation on rainfall. When β is positive, more upwind forest increases rainfall. The identifying assumption in (1) is that changes in upwind forest—driven by land cover and atmospheric transport—are exogenous to other determinants of rainfall.

A concern, especially in the Amazon, is reverse causality: deforestation may respond to rainfall (see Araujo, 2023). We address this in two ways. First, we rely on long-distance transport: most of the variation in upwind forests comes from land-use changes far from the pixels of interest.

Second, we propose an instrumental variable approach that relies solely on year-to-year variation in wind patterns, thereby mitigating the concern that rainfall variation itself may drive changes in forest cover. Since wind is caused by large-scale atmospheric phenomena, such as the difference in atmospheric pressure and the Coriolis effect, forest cover change has no impact on the atmospheric back trajectories (Holton and Hakim, 2013) We construct the instrument $\bar{f}_{it}$ by fixing forest cover at its 1985 level and allowing only atmospheric trajectories to vary:

$$\bar{f}_{it} = \sum_{m} \sum_{j \in B_{imt}} \theta^{s_{mt}(i,j)} p_{j,t=0}.$$

Thus f_{it} incorporates variation in both atmospheric circulation and forest cover from 1985 to 2020, while $\bar{f}_{it}$ varies only with atmospheric circulation. The instrument isolates

[7] We set $\theta = 0.982$ as Araujo (2023), who calibrates this parameter to match the amount of rainfall in the Amazon created by the Amazon itself, a canonical benchmark in the moisture recycling literature (e.g., Zemp et al., 2014; Tuinenburg et al., 2020; Dominguez et al., 2022).

the post-1985 deforestation, with all the identifying variation stemming from changes in high-altitude (i.e., over 2,000 meters) atmospheric transport.

Next, we connect the effect of deforestation on rainfall to river discharge and energy output.

Rainfall on River Discharge. We now map rainfall to river discharge—the volume of water flow per unit of time—at the dam. We use a predictive model to approximate the function that connects rainfall to discharge.[8] Specifically, we model discharge using the following statistical model:

$$\log v_{ht} = c + \gamma \log \left(\sum_{i \in h} r_{it} \right) + \epsilon_{it}, \tag{2}$$

where v_{ht} is the annual mean volumetric discharge at hydropower plant h in year t and $\sum_{i \in h} r_{it}$ is the sum of rainfall in the upstream catchment area of power plant h in year t. The coefficient γ gives the elasticity of river flow to total upstream rainfall.[9]

River Discharge on Energy. Lastly, to connect deforestation to energy, we need a production function of the hydropower plant. We start from the potential gravitational energy equation, which states that $E = m \times$ (gravity acceleration) $\times$ (height), where m is mass. For a hydropower plant, m corresponds to the water mass flowing through its turbines - *i.e.*, its discharge, v_{ht}. Each plant converts a different share, κ_h, of this flow to energy depending on turbine capacity, so potential energy is $E_{ht} = \kappa_h \times v_{ht} \times$ (gravity acceleration) $\times$ (height). This implies a unit-elastic relationship between discharge and energy output.[10] Taking logarithms:

[8] One potential alternative approach would be to use a hydrology model that would account for topography, runoff, and other mechanisms. See, for example, Langevin et al. (2017) for a discussion of the classic MODFLOW model. However, our simpler predictive approach achieves high out-of-sample predictive power, suggesting that the marginal gains from a more complex hydrological specification would be limited for our application.

[9] We experimented with a specification that allows for a discount on distance. In particular we used $\log v_{ht} = c + \theta \log \left(\sum_{i \in h} r_{it} e^{-\lambda \text{dist}(h,i)} \right) + \epsilon_{it}$, where $\text{dist}(h,i)$ denotes the geographical distance between hydropower plant h and pixel i. The introduction of this distance does not improve out-of-sample predictive power. We discuss these results in more detail when we present the empirical results of the model.

[10] When we discuss the empirical results in Section 4.1, we show that we cannot reject that the elasticity is indeed 1.

$$\begin{aligned}\log E_{ht} &= \tilde{c}_h + 1 \times \log v_{ht} \\ &=^{(2)} \tilde{\tilde{c}}_h + \gamma \log\left(\sum_{i \in h} r_{it}\right) + \epsilon_{it},\end{aligned} \tag{3}$$

where the second line substitutes the rainfall-discharge relationship from equation (2).

A potential concern with this approach is that it overlooks the fact that many hydropower plants regulate flows by storing water across seasons. In such cases, inflow does not translate one-to-one into energy generation. However, almost half of Brazil's hydropower generation comes from run-of-river plants, which by design have minimal storage capacity. Additionally, our analysis relies on long-term mean discharge to capture the effect of upstream rainfall on energy output. Storage can smooth out short-term fluctuations, but dams cannot retain water over multi-month periods at the scale required to distort long-term averages. Our empirical data shows exactly this: average inflows and outflows are effectively equal, as shown in Figure B.2.

We have modeled the impact of deforestation on rainfall, of rainfall on river flow, and of river flow on energy potential. We now combine these results to map the impact of deforestation on energy potential.

From Deforestation to Energy. With equations (1), (2), and (3), we can approximate the impact of deforestation on energy as:

$$\begin{aligned}\%\Delta E_{ht} &\approx \gamma \times \%\Delta\left(\sum_{i \in h} r_{it}\right) \\ &= \gamma \times \beta \times \frac{\Delta \sum_{i \in h} f_{it}}{\sum_{i \in h} r_{it}} \\ &= \gamma \times \beta \times \frac{\Delta \sum_{i \in h} \sum_{m} \sum_{j \in B_{imt}} \theta^{s_{mt}(i,j)} p_{jt}}{\sum_{i \in h} r_{it}} \\ &= \gamma \times \beta \times \frac{\sum_{i \in h} \sum_{m} \sum_{j \in B_{imt}} \theta^{s_{mt}(i,j)} \Delta p_{jt}}{\sum_{i \in h} r_{it}}\end{aligned} \tag{4}$$

Equation (4) maps changes in upwind forest cover into relative changes in energy production at the hydropower plant. Given a baseline for the energy potential of each hydropower plant (call it E_{h0}) and a baseline for the rainfall in each pixel (call it r_{i0}) the change in total energy output is given by the sum of changes among all hydropower

plants h:

$$\begin{aligned}\Delta E_t &= \sum_h (\%\Delta E_{ht}) E_{h0} \\ &\approx \gamma \times \beta \times \sum_h \left[\frac{E_{h0}}{\sum_{i \in h} r_{i0}} \times \sum_{i \in h} \sum_m \sum_{j \in B_{imt}} \theta^{s_{mt}(i,j)} \Delta p_{jt} \right]\end{aligned} \tag{5}$$

Equation (5) maps granular changes in forest cover directly to changes in energy production (in GWh) through parameters β and γ. This allows us to simulate electricity-sector outcomes under alternative forest-cover scenarios.

4.1 Results

Deforestation on Rainfall. We start by establishing the causal impact of deforestation on rainfall as described in equation (1). Table 1 shows the results. In the specification with the instrumental variable, a one-standard-deviation increase in upwind forest increases rainfall by 33% of its average. The counterfactual scenarios will offer a more detailed and accurate description of the magnitudes involved in this mechanism. Note that we estimate a single regression for the whole sample—that is, there is one β governing how deforestation affects rainfall on a continental scale. Figure B.1 in the Appendix shows estimates for different samples, with one regression estimated for each large basin. Overall, the coefficients are stable across different samples, especially for the main basins. This means that the causal impact of the Amazon on Brazil's rainfall does not vary substantially across the affected area.

Rainfall on River Flow. Our goal is to predict the effect of rainfall on river discharge for each hydropower plant. We run a five-fold cross-validation exercise, randomizing at the plant level. In each fold, we split the data 80/20 into training and test sets and estimate γ on the training set. We then evaluate the out-of-sample fit of the model in equation (2) with the remaining 20% of observations. This model attains an average R^2 of 0.85 across the five folds. This performance implies that rainfall data yield accurate forecasts of plant-level river flow changes. The elasticity of upriver rainfall on river flow is $\gamma = 0.945$ (standard deviation 0.02, clustering at the plant level): a 1% rise in upriver rainfall predicts a 0.945% increase in discharge. [11]

[11] We also employed a model as $\log v_{ht} = c + \theta \log\left(\sum_{i \in h} r_{it} e^{-\lambda \times \text{dist}(h,i)}\right) + \epsilon_{it}$, where $\text{dist}(h,i)$ is the distance between plant h and pixel i. Figure B.3 (A) reports out-of-sample performance over a range

Table 1: Effect of Upwind Forest on Precipitation

	Dep. Var.: Precipitation	
	OLS	IV
	(1)	(2)
Panel A. Results		
Upwind forest	0.071***	0.119***
	(0.001)	(0.001)
Panel B. First-stage		
Upwind constant forest		0.977***
		(0.001)
F-stat		504,775
Mean Dep.	70.58	70.58
Std Dep.	22.6	22.6
Mean Ind.	280.7	280.7
Std Ind.	195.99	195.99

Notes: Panel A shows the estimates of Equation (1). All specifications include a constant, year, and pixel FEs, and control for upwind exposure to continental land. Column (1) shows OLS estimates of upwind forest on pixel rainfall. Column (2) shows IV estimates of upwind forest on pixel rainfall, where the instrument is the upwind forest keeping forest cover constant at 1985. Panel B shows the first-stage results. Number of observations 408,600. Standard errors are clustered at the pixel level (11,350 clusters). $p^{*} < .10$; $p^{**} < .05$; $p^{***} < .01$.

River Flow on Energy. As described in equation (3), the relation between river flow and energy is not estimated, the elasticity connecting both is one and comes directly from the potential energy equation from physics. Additionally, in Figure B.3 (b) in the Appendix, we show that if we estimate $\log E_{ht} = \alpha_h + \alpha \log r_{ht}$, we cannot reject $\alpha = 1$ in a variety of specifications.

Inference for Deforestation on Energy. We have standard errors for both β and γ, which allows inference on each parameter separately. However, as shown in equation (5), inference on the counterfactual requires the standard error of the product $\beta \times \gamma$. To obtain this, we apply the delta method. In principle, this would require estimating the correlation between β and γ, which is difficult because the two parameters are estimated at different levels of aggregation. We therefore adopt a conservative approach: we bound the standard error from above by assuming a correlation of one between β and

of distance penalties. Including this term does not improve fit and makes the model more complex.

γ.[12] Under this assumption, we obtain a standard error for $\beta \times \gamma$ of 0.002. This value is small, which implies that the standard error of the counterfactual in equation (5) will also be very small. Put differently, even if both β and γ were only marginally significant at the 1% level, the resulting standard error would be 0.04 (0.06 at the 5% level and 0.07 at the 10% level). Hence, concerns about inference do not affect our results in any meaningful way.

5 Conceptual Framework

In this section, we detail the microeconomic framework underlying the welfare analysis. We aim to quantify the welfare gains and redistributive effects of reversing deforestation in the Amazon by increasing water availability in the river basins that supply existing hydropower plants. We employ a standard partial equilibrium model that captures electricity generation and demand within a single market.

Setting. Let the inverse demand function be denoted by $P = D(Q)$, where $D'(\cdot) < 0$, and the inverse supply function by $P = S(Q, R)$, where Q denotes quantity in GWh, P price and R the installed capacity of renewables also in GWh (hydro, wind and solar). We assume that the inverse supply function is increasing in quantity and that renewable power plants produce at zero marginal cost. The initial equilibrium is defined by the intersection of demand and supply for a given renewables capacity R. Let $P_0 = D(Q_0) = S(Q_0, R)$ be the initial market price.

We consider a positive increase in renewables capacity of ΔR. Since renewables face zero marginal cost, this shifts the supply curve outward by ΔR. The new equilibrium quantity Q_1 and price P_1 satisfy: $P_1 = D(Q_1) = S(Q_1, R+\Delta R)$. As $S(\cdot, R)$ is decreasing in renewables capacity, $P_1 < P_0$, that is, more renewables reduce the market energy price.

Welfare analysis. This equilibrium change following the increase in renewables capacity ΔR benefits consumers by reducing electricity prices and increasing quantity demanded:

$$\Delta CS \equiv CS' - CS^* = \int_0^{Q_1} [D(q) - P_1]\, dq - \int_0^{Q_0} [D(q) - P_0] dq \tag{6}$$

[12] The delta method yields $se(\beta \times \gamma) = \sqrt{\hat{\beta}^2 se(\gamma)^2 + 2\rho_{\beta,\gamma}\hat{\gamma}\hat{\beta} se(\beta) se(\gamma) + \hat{\gamma}^2 se(\beta)^2}$. Since $\hat{\beta}, \hat{\gamma} > 0$, setting $\rho_{\beta,\gamma} = 1$ provides an upper bound for the standard error.

$$= \underbrace{(P_0 - P_1)Q_0}_{\text{price gain on old quantity}} + \underbrace{\int_{Q_0}^{Q_1} [D(q) - P_1]\, dq}_{\text{surplus on additional quantity}} \tag{7}$$

Since $P_1 < P_0$ and $D(q) > P_1$ for $q > Q_0$, it follows that $\Delta CS > 0$.

The equilibrium effect on the power sector is captured by the change in producer surplus as follows:

$$\Delta PS = \underbrace{(P_1 - P_0)Q_0}_{\text{price drop on old quantity}} + \underbrace{\int_0^{Q_0} [S(q,R) - S(q,R+\Delta R)]\, dq}_{\text{cost savings on old quantity}} + \underbrace{\int_{Q_0}^{Q_1} [P_1 - S(q,R+\Delta R)]\, dq}_{\text{gain on new quantity}} \tag{8}$$

The first term captures the loss of producer surplus from revenue lost at the baseline quantity produced and it is negative because $P_1 < P_0$. The second term captures cost savings from baseline production as more electricity is generated from zero-marginal-cost renewables. The third term captures gains from increasing the quantity produced. These two former terms are positive. Hence, the sign of the change in producer surplus is ambiguous and depends on whether the sector's cost savings and the gains from production expansion are sufficient to offset the revenue loss from the price decrease. Producer surplus is negative if the loss from a lower price is sufficiently large.

Combining the change in consumer and producer surpluses, we see that the total surplus change of increased renewable capacity is unambiguously positive:

$$\Delta TS = \Delta CS + \Delta PS = \int_0^{Q_0} [S(q,R) - S(q,R+\Delta R)]\, dq + \int_{Q_0}^{Q_1} [D(q) - S(q,R+\Delta R)]\, dq > 0 \tag{9}$$

This is because consumer surplus gains offset all revenue lost by producers, so the net change in total surplus reflects pure efficiency gains from cost reductions and the welfare gains from quantity expansion.

One final element enters the welfare calculation: the change in the externalities from emissions generated by thermal power plants. Consider $e < 0$ the externality imposed by CO2 emissions per GWh of non-renewable electricity production as measured by the social cost of carbon. Then, the welfare change following the expansion of renewables

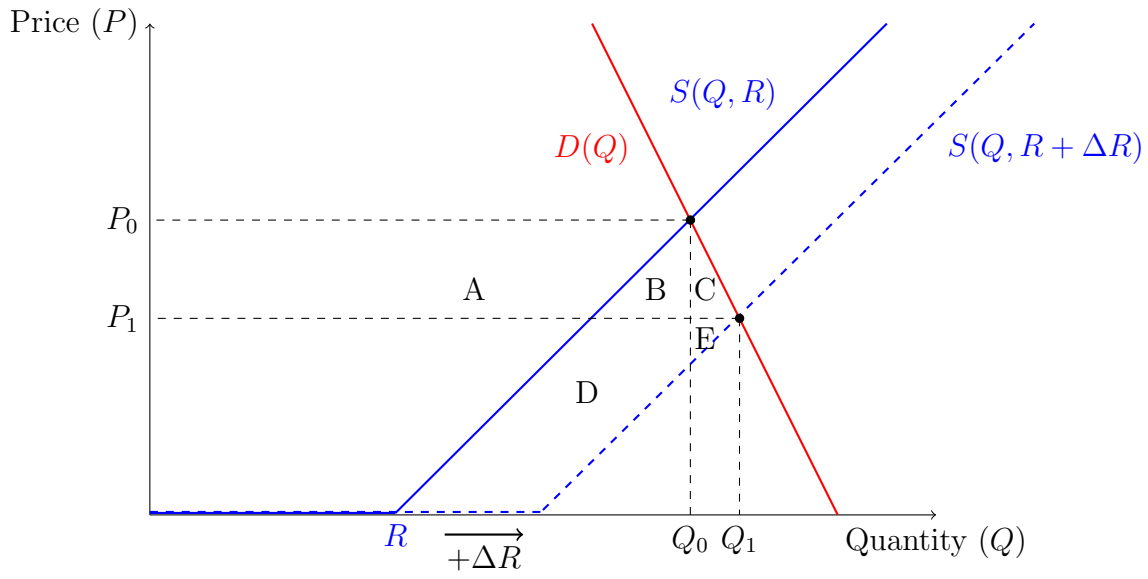
capacity is:

$$\Delta W = \Delta TS + e\left[Q_1 - Q_0 - \Delta R\right] \tag{10}$$

As long as the demand is not perfectly elastic, $Q_1 - Q_0 - \Delta R < 0$, and this last term is positive. This reflects that increased renewable capacity reduces the total non-renewable energy generated in equilibrium.

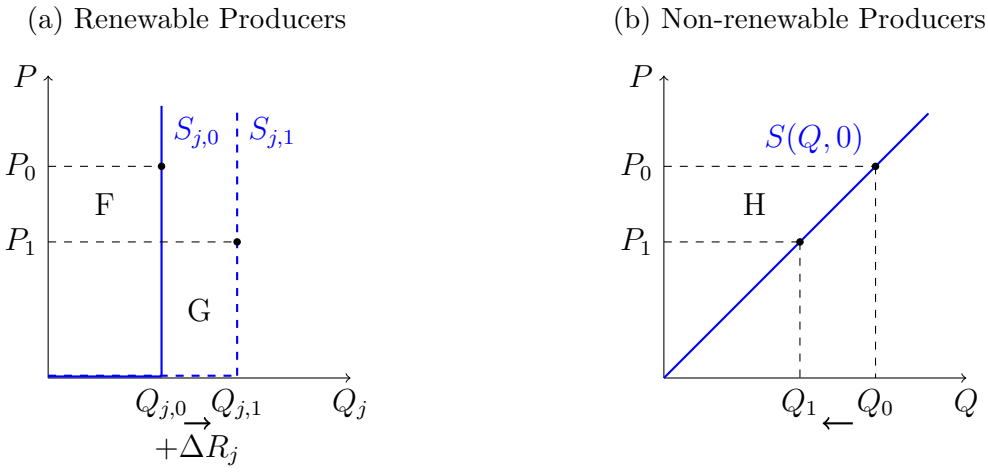
Visualization. Figure 5 presents a simplified version of the model to illustrate the main components of the welfare analysis. The change in consumer surplus corresponds to the price reduction on the initial quantity Q_0 (areas $A+B$) and the consumer surplus from additional energy consumed at the lower price (area C). The change in producer surplus has two components: producers lose surplus due to the price decline (area A), but gain surplus from cost savings and increased quantity (areas $D + E$). The total welfare change is thus represented by the trapezoidal area $B + C + D + E$, plus the additional benefit from reduced emissions.

Figure 5: Welfare Change Following an Increase in Renewables Capacity



Note. This figure illustrates the change in welfare following an increase in renewable capacity from R to $R + \Delta R$. The additional generation capacity shifts the supply curve to the right from $S(Q, R)$ to $S(Q, R + \Delta R)$. As a result, total energy production rises from Q_0 to Q_1 and the market price falls from P_0 to P_1.

Figure 6: Heterogeneous Change in Producer Surplus Following an Increase in Hydro Capacity



Notes: Both figures depict the changes in producer surplus following an increase in hydro capacity that drops prices from P_0 to P_1. (a) Depicts the change in surplus for a renewable producer j that also faces capacity increase ΔR_j, change in surplus: $G - F$. (b) Depicts the change for the non-renewable segment, change in surplus: $-H$.

This simplified diagram, however, hides the heterogeneous effects of this market shift on producers. Figure 6 illustrates the implications of increased hydro capacity for the producer surplus of renewable and non-renewable producers. Panel (a) shows that hydroelectric producers lose surplus F from the price decline on initial quantity but gain G from additional capacity. Whether they gain or lose depends on whether $G > F$. Other renewable producers, wind and solar, only lose surplus F. Panel (b) shows that non-renewable producers unambiguously lose surplus H from facing lower prices and reduced dispatch.

6 Connecting Theory to Data

We have argued that deforestation decreases rainfall and, therefore, hydropower generation capacity. We now study the distributional effects of an increase in energy supply following different reforestation scenarios in Brazil. In this section, we use the partial equilibrium model from Section 5 to quantify the effects of reforestation on the power sector in Brazil. Specifically, we compare hydroelectric output under three counterfactual scenarios: reversing all deforestation since 1985, since 2000, or since 2010, respectively. For each scenario, we use the econometric model in Section 4 to compute

ΔR. We next describe the market assumptions behind our empirical implementation.

Supply. We compute welfare changes using an empirical supply curve built from plant-level operating cost data. For each plant, the National System Operator reports daily operating costs (in R$/MWh) from 2021 to 2024. We deflate costs to January 2020 prices and average them by year to construct four merit-order dispatch curves. Constructing supply curves from merit-order cost information is standard in the empirical electricity literature, where it has been used to measure market power, welfare losses, and the gains from restructuring (Borenstein et al., 2002; Mansur, 2008; Cicala, 2022). We follow this approach to build the supply curve rather than developing a dispatch decision model (as in Gonzales et al., 2023; Jha and Leslie, 2025) because the Brazilian system is centrally operated by the National System Operator, which follows clear merit-order rules. Furthermore, we have the operational costs data that the Operator uses to dispatch generation plants.

To build a single curve for the period, we proceed in two steps. For renewables (hydro, solar, and wind), we assume they operate at zero marginal cost. We use the four-year average output (2021-2024) as a proxy for the average annual generation (in TWh) each source can deliver. [13]

For thermal plants, production incurs positive, rising marginal costs as observed in the official operational costs. To build the supply curve, we take the lower envelope of the four-yearly operating-cost dispatch curves. This corresponds to the cheapest thermal mix observed in the period. This approach is conservative, as most thermal power plants in Brazil operate well below their technical capacity. They serve as the marginal source, activated primarily when renewable generation falls short, and are often shut down for extended periods.

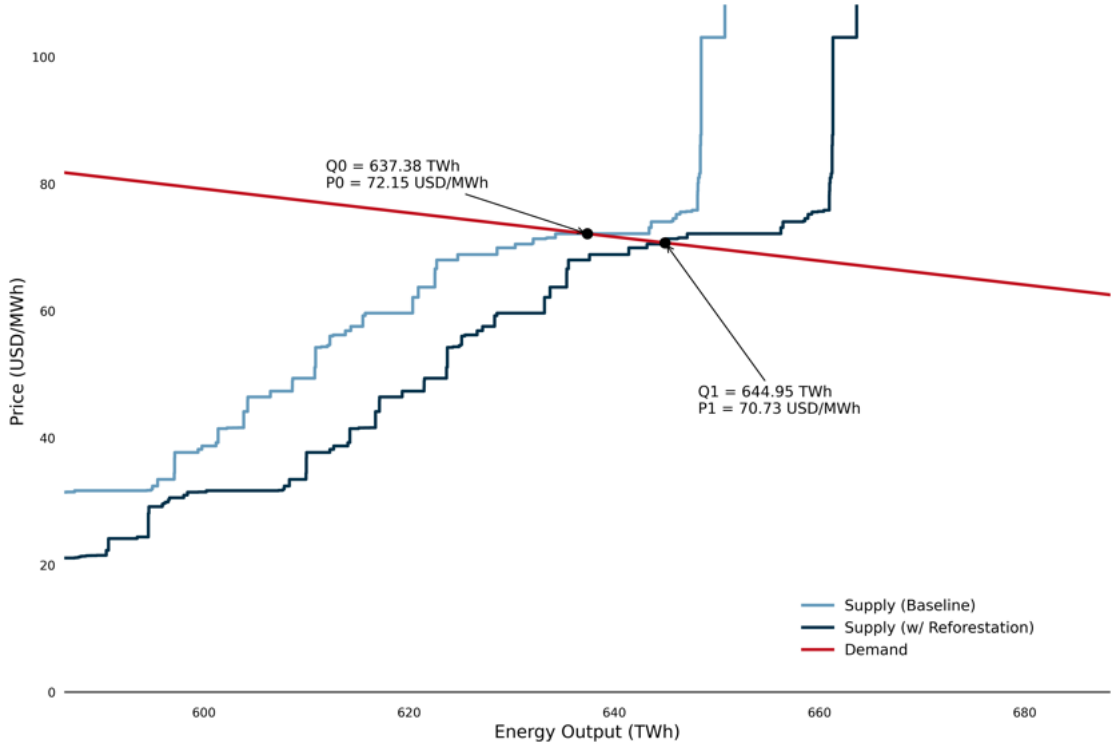
Demand. The last piece we need for our quantification is the demand curve. We do not estimate it directly. Instead, we impose a parametric form and calibrate the elasticity using values from the literature. We consider a linear demand like:

$$P = a - bQ, \quad \text{where} \quad b = \varepsilon_D \frac{P_0}{Q_0}.$$

[13] While hydro installed capacity was stable in this period, this modeling choice understates wind and solar capacity, which grew rapidly in recent years.

We assume a demand-price elasticity $\varepsilon_D = -0.6$ (as in Labandeira et al., 2017) in our main calculations. In Appendix A, we show that using more inelastic elasticities barely changes the welfare effects, but has implications for its distributional effects within the market. Consistent with the construction of the supply curve, we calculate the average electricity demand for 2021-2024 to determine the equilibrium point. In the absence of a structural demand estimate, this provides a conservative benchmark that reflects consumer behavior in recent years.

Figure 7: Empirical Supply and Demand Curves



Notes: This figure illustrates the supply curve shift associated with an increase in hydro supply of 12.8 TWh caused by the counterfactual reforestation of forest cover lost since 1985. The baseline equilibrium is 637.38 TWh at a price of USD 72.15/MWh, while the counterfactual equilibrium reaches 644.95 TWh at USD 70.73/MWh. Original prices are expressed in Jan. 2020 BRL, converted using an exchange rate of 1 USD = 5 BRL. We apply a baseline demand elasticity of –0.6. Because the chart is cropped at 590 TWh, the demand curve may appear more elastic than it actually is.

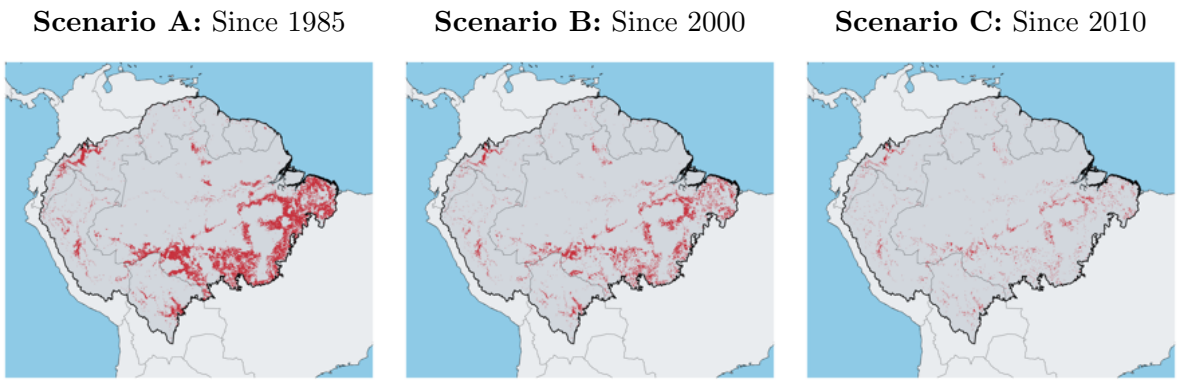
Equilibrium. Because supply must always match demand in electricity markets, we identify the equilibrium quantity by intersecting the average demand curve with the supply curve. Likewise, the demand curve intersects the new supply curve to determine

the new equilibrium point. Figure 7 shows the equilibria under the observed scenario (baseline, Q_0, P_0) and the counterfactual supply curve had we reforested all forest cover lost since 1985 (with reforestation, Q_1, P_1). We present the results from the welfare analysis in the next section.

7 Results

We quantify the welfare costs of deforestation on the Brazilian electricity market by asking how the market would have functioned in 2020 absent the deforestation of recent decades. We consider three scenarios: no deforestation since 1985, since 2000, and since 2010. Figure 8 shows the areas deforested between each base-year and 2020. Total deforestation is 840,000, 435,000, and 170,000 km^2 for each scenario, respectively. The figure also shows different spatial patterns of deforestation over time, with recent deforestation more concentrated along the inner frontier of the Amazon biome in Brazil, commonly known as 'Arc of Deforestation'. For our analysis, the location of deforestation is as important as its scale, because deforestation only affects electricity generation if it occurs upwind from hydropower plants.

Figure 8: Mapping the Reforestation Scenarios



Notes: These maps show the deforested areas in the Amazon between 2020 and 1985 (scenario A), 2000 (scenario B), and 2010 (scenario C) using the data from MapBiomas (2025).

7.1 Rainfall impacts

To construct these counterfactuals, we adopt a similar approach to the one used to build our instrument for estimating the impact of deforestation on rainfall. Specifically,

we fix forest cover at a given year and compute upwind forest exposure using all years of available atmospheric circulation data. We apply this procedure to each counterfactual forest cover year, $C \in \{1985, 2000, 2010\}$, and to the base year of 2020. The underlying assumption is that the 36-year record of atmospheric circulation is representative of atmospheric transport patterns. Therefore, the average upwind forest exposure computed over these years for a given forest cover scenario provides a meaningful estimate of the long-run climatological conditions a planner might expect under that forest cover scenario.

To formalize the counterfactual construction, let $f_{i,t,C}$ denote the upwind forest variable for pixel i computed using the atmospheric circulation of year t and the counterfactual forest cover of year C. We fix forest cover at a reference year C and compute the long-run average upwind forest exposure as:

$$f_i^C = \frac{1}{(36)} \sum_{t=1985}^{2020} f_{i,t,C}.$$

The change in rainfall resulting from reforestation under this counterfactual scenario is then given by:

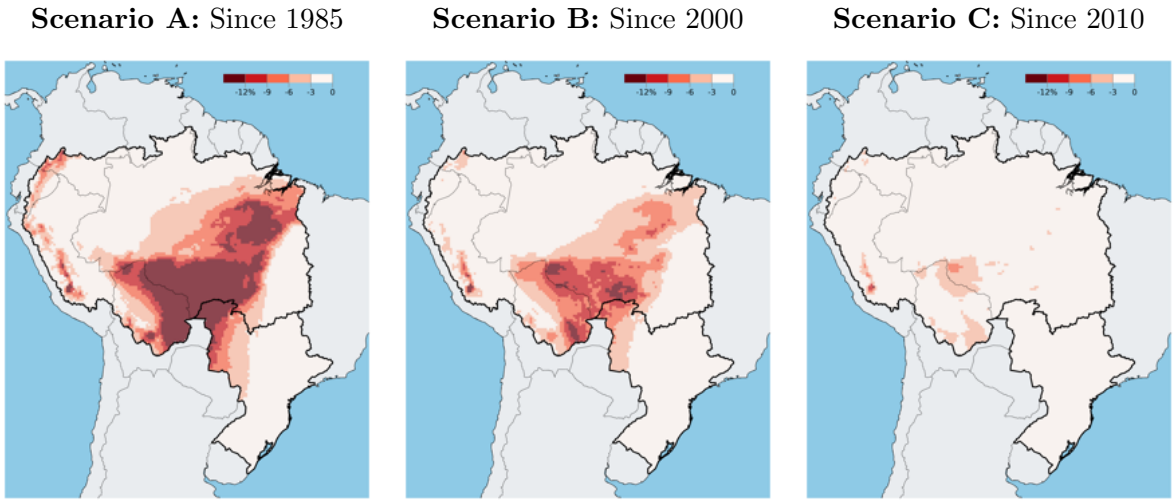
$$\Delta r_i^C = \beta \left(f_i^C - f_i^{2020} \right).$$

As previously discussed, estimating percentage changes in rainfall requires selecting a baseline. While we could use the observed rainfall in 2020 as a baseline, rainfall patterns exhibit substantial year-to-year variation, and our results would be sensitive to whether 2020 had a particularly high or low precipitation level. Ideally, we would observe multiple rainfall realizations with the forest cover of 2020 to compute pixel-level average rainfall. However, this is not feasible, as forest cover changes over time. To mitigate this issue, we take as a base the average observed rainfall for each pixel over the whole sample period, defined as $\bar{r}_i = \frac{1}{36} \sum_{t=1985}^{2020} r_{it}$. This measure is imperfect because it already accounts for the impact of past deforestation on rainfall. Consequently, our baseline rainfall is likely to be overestimated (since early rainfall levels were less affected by deforestation), leading to an underestimation of the percentage change in rainfall and, consequently, an underestimation of the impact of reforestation on energy generation.

Figure 9 displays the resulting spatial change in rainfall under the reforestation scenarios, expressed as a percentage of the baseline $\left(\Delta r_i^C / \bar{r}_i\right)$. It illustrates how much additional rainfall each pixel would receive if all areas deforested since 1985, 2000,

and 2010 were reforested. Under the 1985 forest-cover scenario, some regions would experience rainfall increases of more than 15%. Again, we emphasize that from the perspective of energy generation, the spatial distribution of rainfall matters beyond its magnitude. Reduced rainfall in the upstream areas of large hydropower plants matters much more than reduced rainfall in areas that do not feed any major power plant. Figure 9 also shows that deforestation since 2010 has had little effect on rainfall patterns within Brazilian territory.

Figure 9: Rainfall Losses Under Amazon Deforestation



Notes: These maps show the spatial distribution of the increase in rainfall caused by deforestation since 1985, 2000, and 2010. We limit the scale to 12% for visualization purposes.

7.2 Energy impacts

Equation (5) links forest cover to electricity generation. As with rainfall, we use the average observed energy generation as the baseline. While this approach likely underestimates the true impact of reforestation—since observed generation already reflects the effects of past deforestation—it provides a conservative estimate.

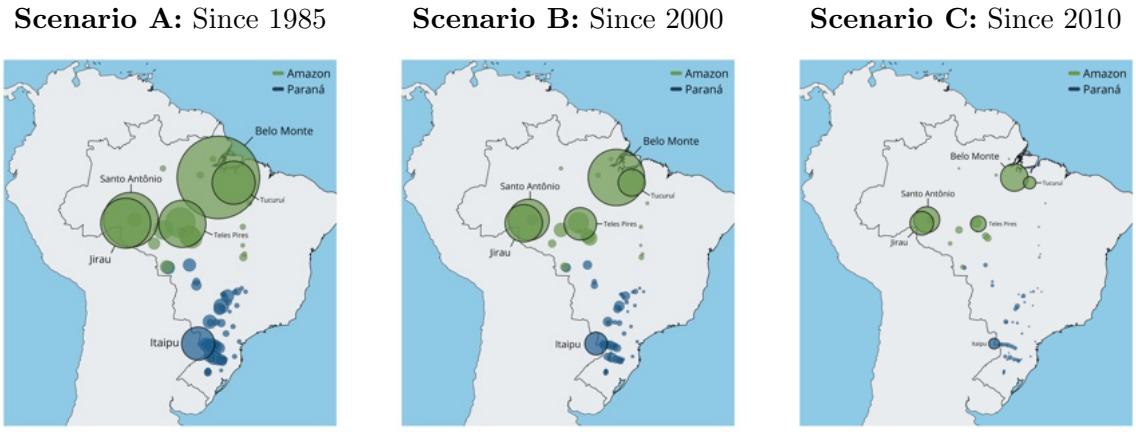
Figure 10 shows the generation gains per hydropower plant under each reforestation scenario. In aggregate terms, deforestation since 1985 (scenario A) has resulted in a total loss of 12.8 TWh of hydropower generation in 2020, corresponding to 3% of average annual hydropower generation.[14] Our results show that 72% of the potential generation

[14]This average is of 420 TWh of hydroelectricity between 2021 and 2024.

gain from reforestation would be concentrated in six hydropower plants: Belo Monte, Santo Antônio, Jirau, Tucuruí, Teles Pires, and Itaipu (the only one not in the Amazon River basin).

We calculate that the cumulative losses for deforestation since 2000 and since 2010 are 6.2 TWh and 1.7 TWh, respectively, corresponding to 1.5% and 0.4% of average annual hydro generation. The spatial concentration pattern is similar across scenarios, with the same six plants accounting for the majority of impacts.

Figure 10: Energy Gains per Hydropower Plant Under Amazon Reforestation Scenarios



Notes: These maps illustrate increase in hydroelectric generation under three reforestation scenarios. In each case, we highlight the six hydropower plants that benefit the most from reforestation: Belo Monte, Santo Antônio, Jirau, Itaipu, Tucuruí and Teles Pires. Together, these power plants account for, 72%, 73% and 77% of the total gains in the 1985, 2000 and 2010 scenarios, respectively. Green and blue shades represent hydropower plants in the Amazon and Paraná riven basins, respectively.

7.3 Welfare analysis

We now quantify the welfare value of the forest to the Brazilian electricity market. The framework in Section 5 shows that while total welfare is increasing in Amazon forest cover, primarily through consumer gains, the effects on producers are ambiguous, with some producers potentially worse off from reforestation. As described in Section 6, we apply the model to compute the welfare and distributional effects of Amazon reforestation.

Table 2 shows the welfare decomposition for the three reforestation scenarios. The first row confirms that consumer surplus increases with reforestation in all scenarios. As shown in Figure 7, reforestation increases rainfall and hydro generation, reducing re-

Table 2: Welfare Impacts of an Increase in Hydroelectric Capacity (million USD)

Scenario	1985	2000	2010
Δ Consumer Surplus	916.1	379.3	3.9
Δ Producer Surplus	4.1	71.4	121.2
Solar and Wind	-174.8	-72.5	-0.8
Hydro	308.2	198.2	122.5
Amazon	543.5	285.4	104.7
Parana	-125.2	-41.6	18.2
Other	-110.1	-45.7	-0.5
Thermal	-129.4	-54.3	-0.6
Δ Total Surplus (PS + CS)	920.2	450.7	125.1
Δ Thermal Carbon Cost	175.5	103.4	56.6
Δ Welfare	1095.7	554.1	181.7

Notes: This table shows the welfare changes in the Brazilian electricity sector for the three scenarios: full reforestation of deforested areas since 1985, 2000, and 2010, respectively. We consider a demand elasticity of $e = -0.6$ and an exchange rate of 1 USD = 5 BRL.

liance on expensive thermal plants, lowering electricity prices, and increasing electricity consumption.

Table 2 column 1 shows that all forest cover lost since 1985 would increase hydro generation and lower prices sufficiently to generate consumer surplus gains of 916 million USD per year. This corresponds to approximately 20% of the annual subsidies Brazilian electricity consumers pay.[15] Column 2 shows that forests lost between 2000 and 2020 account for about one-third of these consumer gains. In the 2010 scenario (column 3), the smaller increase in hydro output results in minimal price effects and consumer welfare gains of only 3.9 million USD per year.

Producer surplus also increases with reforestation in all scenarios, rising by only 4.1 million USD per year under the 1985 scenario and by 121 million USD in the 2010 scenario. However, producer welfare changes vary substantially across generation technologies and plant locations.

Hydroelectric producers gain 308 million USD per year from restoring the 1985 forest

[15]The CDE (*Conta de Desenvolvimento Energético*) is a sector-wide charge collected through electricity bills to fund policy subsidies and sector charges. In 2020, the CDE totaled 4,400 million USD.

cover. This is because the increase in hydro plant output dominates the price reduction in aggregate terms. However, gains vary substantially across river basins. Amazon Basin plants experience the largest output increases, gaining a combined surplus of 543 million USD. The Paraná Basin plants lose USD 125 million per year because the price drop outweighs the gains from increased rainfall. The remaining basins lose USD 110 million in that same scenario as they just face a decreased price, since they are not affected the Amazon moisture flows.

Other generation technologies also lose. Solar and wind producers remain fully dispatched as their marginal costs stay below the market-clearing price, but lose 175 million USD in the 1985 scenario due to the price decline under greater reforestation. Thermal producers lose 130 million USD due to reforestation as they are dispatched less frequently because of increased hydro output and face lower prices.

This result shows that producer gains are concentrated in power plants located in the Amazon basin, which experience the largest rainfall losses from deforestation. Power plants in the rest of the country incur net losses under large-scale reforestation, including even those in the Paraná basin that receive moisture flows originating in the Amazon. For all these plants, price losses outweigh any potential benefits (if any). This pattern explains why the change in producer surplus declines with reforestation, going from USD 4 million under the large-scale reforestation scenario in 1985 to USD 121 million under the limited reforestation scenario in 2010.

In total, the change in total surpluses (consumer plus producer) amounts to 920 million USD per year under the 1985 scenario. Reforesting all forests lost since 2000 (scenario B) would create total surplus gains of 450 million USD per year, about half the magnitude of scenario A. A more modest scenario, reforesting just areas deforested since 2010, would increase total surpluses by 125 million USD per year.

Reforestation also provides environmental benefits beyond these market effects. Increasing renewable generation capacity reduces emissions from thermal generation. We compute a back-of-the-envelope estimate of the carbon externality using a social cost of carbon of 50 USD per tCO2 and emissions of 665.4 tCO2 per GWh of thermal electricity (IEMA, 2024). Based on this calculation, reduced thermal emissions from reforesting areas lost since 1985 are worth 175 million USD annually.

The total welfare gains from restoring forest cover to 1985 levels are thus 1.1 billion USD per year. Restoring 2000 or 2010 forest cover yields 554 million and 182 million USD per year, respectively. As a benchmark, the net revenue of the Brazilian electricity

market in 2020 was 35.2 billion USD,[16] so yearly social gains in the most ambitious reforestation scenario amount to about 3% of annual sector revenue. At a 5% discount rate, the present value of these annual gains are 21.9 billion, 11.1 billion, and 3.7 billion USD across the three scenarios. These figures represent the social value of forest loss from the perspective of energy markets, and serve as the foundation for a granular targeting exercise in the next section.

7.4 Targeting Conservation and Reforestation

While reforesting all areas cleared since 1985, 2000, or 2010 is not feasible, policies targeting conservation and reforestation in high social value or high-pressure areas are common and central to the policy debate (e.g., Assunção et al., 2023). We now assess whether targeted conservation and reforestation can deliver substantial gains in rainfall and hydropower generation. Equation 5 links forest cover to hydropower output, assigning an energy value to the forest as a whole. Using the same estimated parameters and upwind relationships, we can assign an energy value to each pixel in the region, independently of its current land use.

To construct this metric, for each pixel j, we identify the set D_{jmt} of downwind pixels at a given month m and year t. Because we know how rainfall at each downwind pixel $i \in D_{jmt}$ affects hydropower production, we can trace how each forest pixel contributes to energy output at each hydropower h. The contribution of full forest cover in pixel j to rainfall at downwind pixel i is given by $\beta\theta^{s_{mt}(i,j)}$. In turn, the average output of rainfall for hydropower h is given by $E_{h,0}/\sum_{\ell\in h} r_{\ell,0}$.[17] Thus, we compute the average contribution of the forest in pixel j to hydroelectric generation by summing this combined effect for all pixels downwind of j:

$$E_{jmt} = \sum_{i\in D_{jmt}} \beta\theta^{s_{mt}(i,j)} \times \frac{E_{h(i),0}}{\sum_{\ell\in h(i)} r_{\ell,0}}, \tag{11}$$

where $h(i)$ is the power plant whose catchment area includes i.

We average E_{jmt} across all months from 1985 to 2020 to obtain the mean energy contribution of full forest cover in pixel j. We then assign each pixel a monetary value proportional to its contribution, scaled so that reforesting all areas lost between 1985

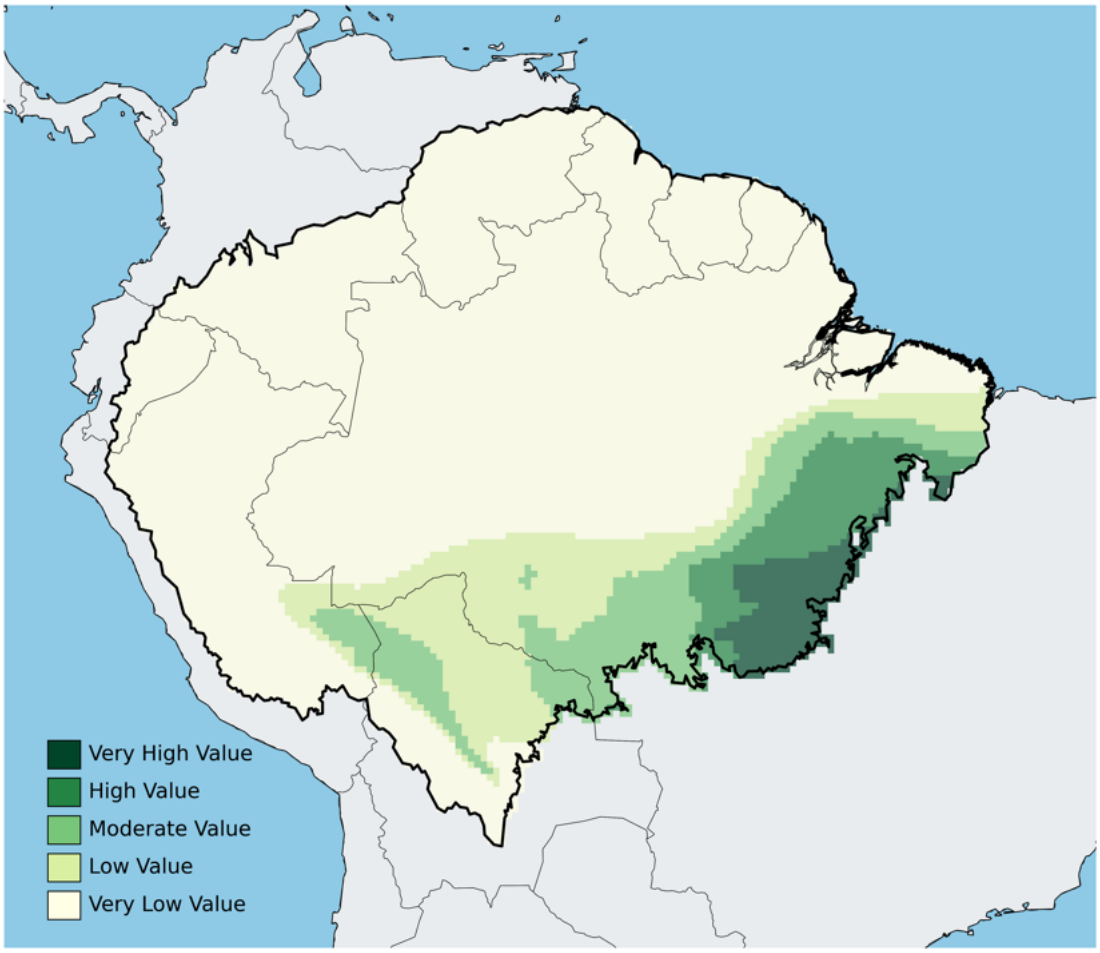
[16] We proxy the sector's revenue by the regulated revenue requirement (*receita requerida*, *Informativo de Gestão do Setor Elétrico – Ano 2020* MME/DGSE).

[17] As in equation 5, we need reference baselines power output for h, $E_{h,0}$, and total rainfall in pixels upstream of h, $\sum_{\ell\in h} r_{\ell,0}$. We use the same baseline values as in the main counterfactual scenarios.

and 2020 yields $21.9 billion USD—the present value of total welfare gain from that scenario. We provide further details on this calculation in Appendix C. The result is a granular map of forest value, denominated in electricity market welfare contributions.

We find that these values are highly unevenly distributed across the Amazon: not all areas contribute equally to energy security. Figure 11 maps the spatial distribution of forests' energy value. Each of the five colored areas represents forest areas worth 23 billion USD. The highest-value region, covering only 3.3% of the area, accounts for 20% of the forest's total energy value.

Figure 11: The Energy Value of the Amazon



Notes: This figure shows the monetary value of Amazon forests for Brazilian electricity generation under the 1985 reforestation scenario. Each pixel's value depends on the distance to downwind areas, the rainfall it generates downwind, and the hydropower generated from that rainfall. The five colored regions represent equal-value quintiles (23 billion USD each).

The results highlight the 'Arc of Deforestation'—the region of most intense recent forest loss driven by the expansion of the agricultural frontier—as critical for hydropower. This area encompasses much of the Amazon, where numerous upwind trajectories that transport moisture to large hydropower plants pass through. Notably, these high-value areas also include prominent indigenous territories under pressure to downsize or downgrade their protection status. For example, forests in the Xingu Indigenous Park alone are worth roughly USD 5 billion in hydropower value, making their protection an efficient policy that enhances both energy security and social welfare.

In contrast, preserving the deeper Amazon, which has experienced less deforestation, has a more limited effect on rainfall relevant to electricity generation. Trajectories passing through these areas do not reach many upstream regions of hydropower plants. This does not imply that these areas do not contribute to rainfall (they contribute substantial amounts) but rather that the rainfall from these regions contributes less to hydropower production due to the mismatch between power plants' catchment areas and wind patterns.

This pattern contrasts with priority regions identified for other ecosystem services. Areas with the highest carbon stocks (Baccini et al., 2012) and for maintaining forest stability and avoiding potential tipping point are located deeper within the forest (Araujo et al., 2023; Flores et al., 2024). Biodiversity priorities likewise highlight other portions of the basin (Jenkins et al., 2013). These differences highlight the importance of accounting not only for the spatial distribution of forests and their evapotranspiration potential, but also for the full chain linking atmospheric moisture recycling to river flows at hydropower plants, together with the heterogeneous location and scale of hydropower infrastructure.

8 Conclusions

We study the impact of Amazon deforestation on the Brazilian power sector. First, we model how forest loss reduces electricity supply. We then quantify the welfare effects on consumers, producers, and the economy as a whole caused by deforestation in the Amazon. Finally, we map the Amazon areas most critical for sustaining hydropower generation.

Our main result is that deforestation generates net gains for the power sector, except for those hydropower plants directly affected by reduced rainfall. Lower precipitation caused by deforestation reduces hydroelectric output but sustains higher electricity

prices for many producers. The net gains are particularly strong for thermal plants and other renewable producers that face no or small direct effects from reduced rainfall, which benefit from both higher dispatch and higher prices. By contrast, consumers always lose surplus due to the reduced availability of cheap hydroelectricity. The larger the deforested area, the more pronounced the effects. We also identify the Amazon areas most critical for rainfall relevant to hydropower.

We acknowledge that our model is not perfect. We thus adopt restrictive assumptions to make our estimates conservative. That is, our estimates likely understate the true effects of deforestation on the Brazilian power market.

These findings have two direct policy implications. First, conservation policy and energy policy are complements. For countries that rely on hydropower and face pressure to convert forested land, protecting forests raises the returns to clean energy investment. Ignoring this linkage understates the benefits of conservation and leads to underinvestment in forest protection. Second, our framework provides a tool to assess the welfare and distributional impacts of supply shifts in electricity markets more broadly—whether driven by environmental change or the energy transition. While such changes may raise total welfare, they generate uneven gains and losses across market participants, and our approach traces these distributional consequences.

For Brazil specifically, our results quantify the externality of Amazon deforestation on the power sector, which adds to the well-known costs of carbon emissions, biodiversity loss, and agricultural productivity. By mapping where preservation is most valuable, we offer guidance for spatially targeted conservation and restoration when policy aims to safeguard electricity supply.

References

Araujo, R. (2023). When clouds go dry: An integrated model of deforestation, rainfall, and agriculture. *Working paper*.

Araujo, R. (2024). The value of tropical forests to hydropower. *Energy Economics 129*, 107205.

Araujo, R., J. Assunção, M. Hirota, and J. A. Scheinkman (2023). Estimating the spatial amplification of damage caused by degradation in the amazon. *Proceedings of the National Academy of Sciences 120*(46), e2312451120.

Araujo, R., F. Costa, and M. Sant'Anna (2026). Efficient conservation of the brazilian

amazon: Estimates from a dynamic model. *Review of Economic Studies 93*(1), 72–105.

Arrow, K., P. Dasgupta, L. Goulder, G. Daily, P. Ehrlich, G. Heal, S. Levin, K.-G. Mäler, S. Schneider, D. Starrett, et al. (2004). Are we consuming too much? *Journal of Economic Perspectives 18*(3), 147–172.

Assunção, J., R. McMillan, J. Murphy, and E. Souza-Rodrigues (2023). Optimal environmental targeting in the amazon rainforest. *Review of Economic Studies 90*(4), 1608–1641.

Assunção, J. J., L. P. Hansen, T. Munson, and J. Scheinkman (2023). Carbon prices and forest preservation over space and time in the brazilian amazon. *Becker Friedman Institute for Economics Working Papers Series*.

Baccini, A., S. J. Goetz, W. Walker, N. Laporte, M. Sun, D. Sulla-Menashe, J. Hackler, P. Beck, R. Dubayah, M. Friedl, et al. (2012). Estimated carbon dioxide emissions from tropical deforestation improved by carbon-density maps. *Nature climate change 2*(3), 182–185.

Balboni, C. (2025). In harm's way? infrastructure investments and the persistence of coastal cities. *American Economic Review 115*(1), 77–116.

Balboni, C., A. Berman, R. Burgess, and B. A. Olken (2023). The economics of tropical deforestation. *Annual Review of Economics 15*, 723–754.

Besley, T. and T. Persson (2023). The political economics of green transitions. *Quarterly Journal of Economics 138*(3), 1863–1906.

Borenstein, S., J. B. Bushnell, and F. A. Wolak (2002). Measuring market inefficiencies in California's restructured wholesale electricity market. *American Economic Review 92*(5), 1376–1405.

Borenstein, S. and R. Kellogg (2023). Carbon pricing, clean electricity standards, and clean electricity subsidies on the path to zero emissions. *Environmental and Energy Policy and the Economy 4*(1), 125–176.

Brander, J. A. and M. S. Taylor (1998). The simple economics of easter island: A ricardo-malthus model of renewable resource use. *The American Economic Review 88*(1), 119–138.

Bruno, E. M. and K. Jessoe (2021). Missing markets: Evidence on agricultural groundwater demand from volumetric pricing. *Journal of Public Economics 196*, 104374.

Butters, R. A., J. Dorsey, and G. Gowrisankaran (2025). Soaking up the sun: Battery investment, renewable energy, and market equilibrium. *Econometrica 93*(3), 891–927.

Cicala, S. (2022). Imperfect markets versus imperfect regulation in US electricity generation. *American Economic Review 112*(2), 409–441.

Copernicus Climate Change Service (C3S) (2017). Era5: Fifth generation of ecmwf atmospheric reanalyses of the global climate. https://cds.climate.copernicus.eu/datasets/reanalysis-era5-single-levels?tab=download. Accessed on July 2025.

Costa, F., A. Hsiao, H. Pellegrina, and E. Souza-Rodrigues (2025). Deforestation. *VoxDevLit*.

Costanza, R., R. d'Arge, R. De Groot, S. Farber, M. Grasso, B. Hannon, K. Limburg, S. Naeem, R. V. O'neill, J. Paruelo, et al. (1997). The value of the world's ecosystem services and natural capital. *Nature 387*(6630), 253–260.

Costinot, A., D. Donaldson, and C. Smith (2016). Evolving comparative advantage and the impact of climate change in agricultural markets: Evidence from 1.7 million fields around the world. *Journal of Political Economy 124*(1), 205–248.

Currie, J. and R. Walker (2019). What do economists have to say about the Clean Air Act 50 years after the establishment of the Environmental Protection Agency? *Journal of Economic Perspectives 33*(4), 3–26.

Dominguez, F., J. Eiras-Barca, Z. Yang, D. Bock, R. Nieto, and L. Gimeno (2022). Amazonian moisture recycling revisited using wrf with water vapor tracers. *Journal of Geophysical Research: Atmospheres 127*(4), e2021JD035259.

Domínguez-Iino, T. (2026). Efficiency and redistribution in environmental policy: An equilibrium analysis of agricultural supply chains. *Journal of Political Economy*, 000–000.

Ember (2025). Yearly Electricity Data. https://ember-energy.org/data/yearly-electricity-data/. Accessed on July 2025.

Eva, H. D., O. Huber, and European Communities (2005). *A proposal for defining the geographical boundaries of Amazonia*. Luxembourg: Publications Office.

Fabra, N. and G. Llobet (2025). Designing contracts for the energy transition. *International Journal of Industrial Organization 102*, 103173.

Farrokhi, F., E. Kang, H. S. Pellegrina, and S. Sotelo (2025). Deforestation: A global and dynamic perspective. Technical report, National Bureau of Economic Research.

Ferguson, B. (2024). Trade frictions in surface water markets. *Working paper*.

Ferraro, P. J., K. Lawlor, K. L. Mullan, and S. K. Pattanayak (2012). Forest figures: Ecosystem services valuation and policy evaluation in developing countries. *Review of Environmental Economics and Policy 6*(1), 20–44.

Flores, B. M., E. Montoya, B. Sakschewski, N. Nascimento, A. Staal, R. A. Betts, C. Levis, D. M. Lapola, A. Esquível-Muelbert, C. Jakovac, et al. (2024). Critical transitions in the amazon forest system. *Nature 626*(7999), 555–564.

Frank, E. G. and K. Oremus (2025). Regulating biological resources: lessons from marine fisheries in the united states. Technical report, National Bureau of Economic Research.

Gernaat, D. E., P. W. Bogaart, D. P. v. Vuuren, H. Biemans, and R. Niessink (2017). High-resolution assessment of global technical and economic hydropower potential. *Nature Energy 2*(10), 821–828.

Gonzales, L. E., K. Ito, and M. Reguant (2023). The investment effects of market integration: Evidence from renewable energy expansion in chile. *Econometrica 91*(5), 1659–1693.

Gowrisankaran, G., A. Langer, and M. Reguant (2024). Energy transitions in regulated markets. Technical report, National Bureau of Economic Research.

Grosset, F., A. Papp, and C. Taylor (2023). Rain follows the forest: Land use policy, climate change, and adaptation. *Working paper*.

Hausman, C. (2025). Power flows: Transmission lines, allocative efficiency, and corporate profits. *American Economic Review 115*(8), 2574–2615.

Holton, J. R. and G. J. Hakim (2013). *An Introduction to Dynamic Meteorology* (5 ed.). Amsterdam: Academic Press.

Hsiao, A. (2023). Sea level rise and urban adaptation in jakarta. *working paper*.

IEMA (2024). 4º inventário de emissões atmosféricas em usinas termelétricas: Geração de eletricidade, emissões e lista de empresas proprietárias das termelétricas a combustíveis fósseis do sistema interligado nacional (ano-base 2023). Technical report, Instituto de Energia e Meio Ambiente. Acessed on August 2025.

Ito, K. (2025). Renewable energy expansion: Key challenges and emerging opportunities. In *Advances in Economics and Econometrics: Twelfth World Congress of the Econometric Society*.

Jenkins, C. N., S. L. Pimm, and L. N. Joppa (2013). Global patterns of terrestrial vertebrate diversity and conservation. *Proceedings of the National Academy of Sciences 110*(28), E2602–E2610.

Jha, A. and G. Leslie (2025). Start-Up Costs and Market Power: Lessons from the Renewable Energy Transition. *American Economic Review 115*(2), 690–724.

Labandeira, X., J. M. Labeaga, and X. López-Otero (2017). A meta-analysis on the price elasticity of energy demand. *Energy Policy 102*, 549–568.

Langevin, C. D., J. D. Hughes, E. R. Banta, R. G. Niswonger, S. Panday, and A. M. Provost (2017). Documentation for the modflow 6 groundwater flow model. Technical report, US Geological Survey.

Lehner, B. and G. Grill (2013). Global river hydrography and network routing: baseline data and new approaches to study the world's large river systems. *Hydrological Processes 27*(15), 2171–2186.

Mansur, E. T. (2008). Measuring welfare in restructured electricity markets. *The Review of Economics and Statistics 90*(2), 369–386.

MapBiomas (2025). Coleção 9 da série anual de mapas de cobertura e uso da terra do brasil. https://brasil.mapbiomas.org/colecoes-mapbiomas/. Accessed on July 2025.

Marengo, J. A., C. M. Souza, K. Thonicke, C. Burton, K. Halladay, R. A. Betts, L. M. Alves, and W. R. Soares (2018). Changes in climate and land use over the amazon region: Current and future variability and trends. *Frontiers in Earth Science 6*, 228.

Nordhaus, W. (2019). Climate change: The ultimate challenge for economics. *American Economic Review 109*(6), 1991–2014.

Operador Nacional do Sistema Elétrico (ONS) (2025a). Capacidade instalada de geração. https://dados.ons.org.br/dataset/capacidade-geracao. Accessed on July 2025.

Operador Nacional do Sistema Elétrico (ONS) (2025b). Cvu das usinas térmicas. https://dados.ons.org.br/dataset/cvu-usitermica. Accessed on July 2025.

Operador Nacional do Sistema Elétrico (ONS) (2025c). Dados hidrológicos por reservatório - base diária. https://dados.ons.org.br/dataset/dados-hidrologicos-res. Accessed on July 2025.

Operador Nacional do Sistema Elétrico (ONS) (2025d). Geração por usina em base horária. https://dados.ons.org.br/dataset/geracao-usina-2. Accessed on July 2025.

Pfafstetter, O. (1989). *Classificação de Bacias Hidrográficas – Metodologia de Codificação*. Rio de Janeiro, RJ: Departamento Nacional de Obras de Saneamento (DNOS).

Ryan, N. and A. Sudarshan (2022). Rationing the commons. *Journal of Political Economy 130*(1), 210–257.

Salati, E., A. Dall'Olio, E. Matsui, and J. R. Gat (1979). Recycling of water in the Amazon Basin: An isotopic study. *Water Resources Research 15*(5), 1250–1258.

Smith, C., J. C. A. Baker, and D. V. Spracklen (2023). Tropical deforestation causes large reductions in observed precipitation. *Nature 615*(7951), 270–275.

Souza-Rodrigues, E. (2019). Deforestation in the amazon: A unified framework for estimation and policy analysis. *Review of Economic Studies 86*(6), 2713–2744.

Spracklen, D. V., S. R. Arnold, and C. M. Taylor (2012). Observations of increased tropical rainfall preceded by air passage over forests. *Nature 489*(7415), 282–285.

Stickler, C. M., M. T. Coe, M. H. Costa, D. C. Nepstad, D. G. McGrath, L. C. Dias, H. O. Rodrigues, and B. S. Soares-Filho (2013). Dependence of hydropower energy generation on forests in the amazon basin at local and regional scales. *Proceedings of the National Academy of Sciences 110*(23), 9601–9606.

Tol, R. S. (2023). Social cost of carbon estimates have increased over time. *Nature Climate Change 13*(6), 532–536.

Tuinenburg, O. A., J. J. Theeuwen, and A. Staal (2020). High-resolution global atmospheric moisture connections from evaporation to precipitation. *Earth System Science Data Discussions 2020*, 1–24.

Wunderling, N., A. Staal, B. Sakschewski, M. Hirota, O. A. Tuinenburg, J. F. Donges, H. M. J. Barbosa, and R. Winkelmann (2022). Recurrent droughts increase risk of cascading tipping events by outpacing adaptive capacities in the Amazon rainforest. *Proceedings of the National Academy of Sciences 119*(32), e2120777119.

Zemp, D., C.-F. Schleussner, H. Barbosa, R. Van Der Ent, J. F. Donges, J. Heinke, G. Sampaio, and A. Rammig (2014). On the importance of cascading moisture recycling in south america. *Atmospheric Chemistry and Physics 14*(23), 13337–13359.

Appendix (for online publication)

A Elasticity Robustness

In this section, we discuss the role of the demand elasticity in our results. On the baseline scenario, we consider it to be $e = -0.6$, as Labandeira et al. (2017) suggests for the long-term elasticity demand for electricity.

However, electricity is generally considered an inelastic good. In the following charts, we show how prices, quantities, surpluses, and welfare change under different elasticities. For all of them, we run the model with $e \in [-1, 1)$, for 0.01 steps and consider the three reforestation scenarios (1985, 2000, and 2010).

In Figure A.1, we show how the consumer surplus changes for multiple elasticities in the three scenarios. It generally increases more under low elasticity, as the positive hydro shock translates into larger price drops. This is necessary for market clearing, and consumers do benefit from it.

As in 2010, there is no price change due to the limited gain in energy, and there is no change in the consumer surplus. In the other two scenarios, where reforestation results in price drops, the CS gain is bigger and the demand is more inelastic.

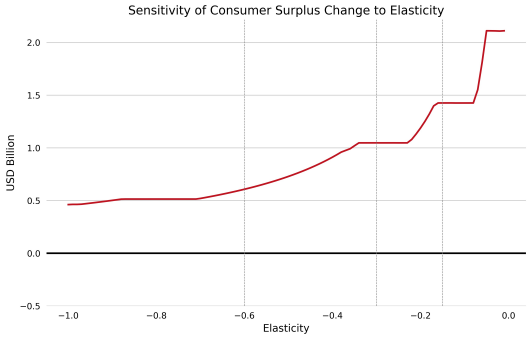
We also investigate the impact of demand elasticity on changes in producer surplus (PS). More inelastic demand leads to larger price drops, which affects consumers differently. Figure A.2 suggests that on the 1985 and 2010 scenarios, inelastic demand actually hurts the producers. That is mainly due to the fact that it changes the sign of the PS change for hydropower plants. With large elasticity, the extra hydropower from reforestation is consumed with almost no drop in price. Under inelasticity, it is also consumed but with a large drop in price, thus leading to the surplus lost shown in Figure A.3.

As it happens, with the change in consumer surplus, these results do not apply to the 2010 scenario. Again, since there is no price change, the welfare change is limited to the gains from extra energy sold. For hydro, the extra 1.3TWh is sold at the same price for all elasticities, that is why a straight line.

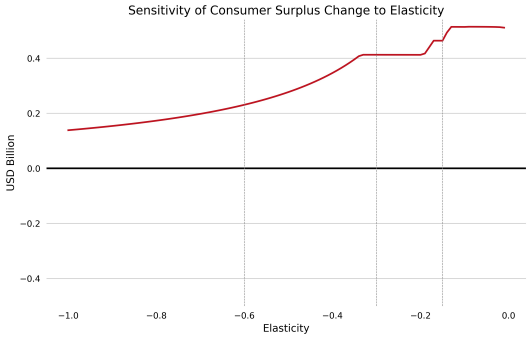
In aggregate terms, how does elasticity impact the total welfare? Figure A.5 shows that the consumer gains outweigh the producers' losses as demand becomes inelastic.

Figure A.1: Impact of the Demand Elasticity on Consumer Surplus Change

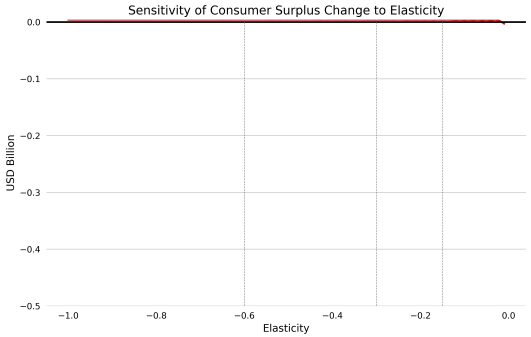
Scenario A: 1985



Scenario B: 2000



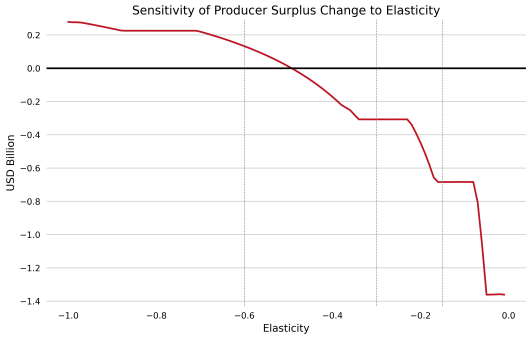
Scenario C: 2010



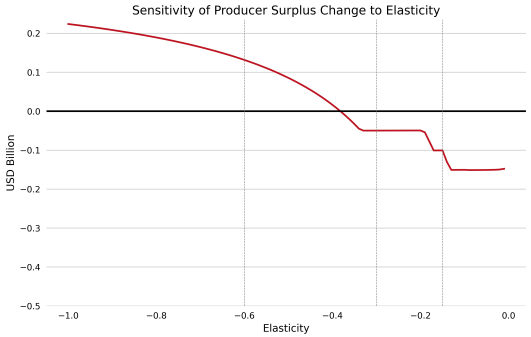
Notes: These charts show the impact of using different demand elasticities on Δ Consumer Surplus (CS) in the 1985, 2000 and 2010 reforestation scenario. In both charts, $e \in \{-0.6, -0.3, -0.1\}$ are highlighted with vertical lines.

Figure A.2: Impact of the Demand Elasticity on Producer Surplus Change

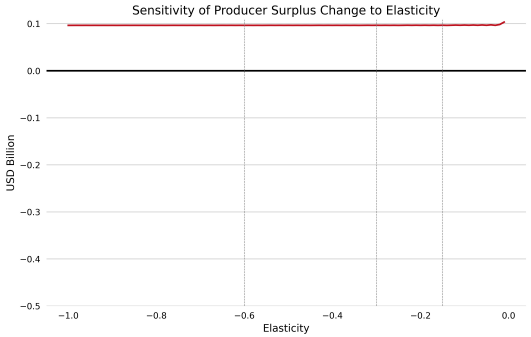
Scenario A: 1985



Scenario B: 2000



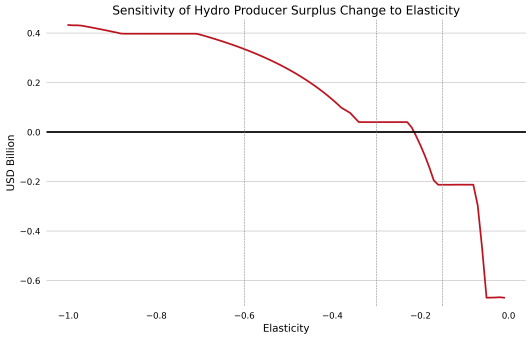
Scenario C: 2010



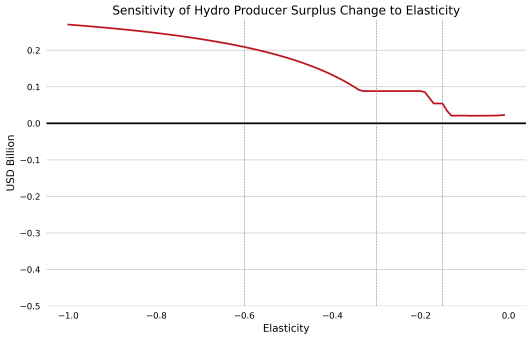
Notes: These charts show the impact of using different demand elasticities on Δ Producer Surplus (PS) in the 1985, 2000 and 2010 reforestation scenario. In both charts, $e \in \{-0.6, -0.3, -0.1\}$ are highlighted with vertical lines.

Figure A.3: Impact of the Demand Elasticity on Hydro Producer Surplus Change

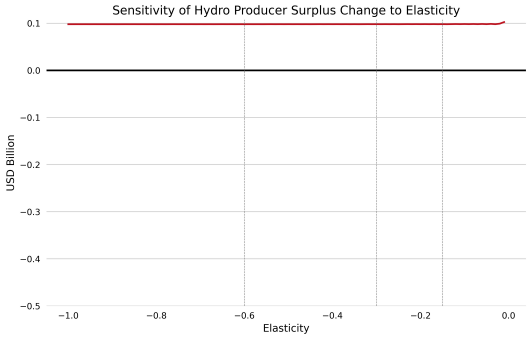
Scenario A: 1985



Scenario B: 2000



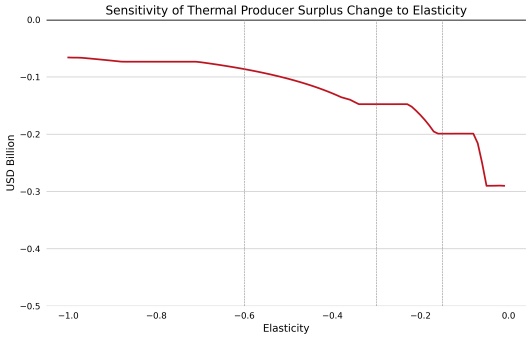
Scenario C: 2010



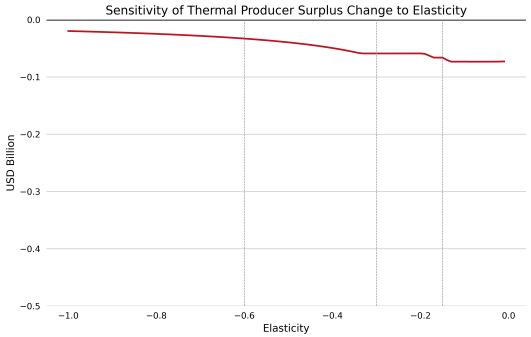
Notes: These charts show the impact of using different demand elasticities on Δ Hydro Producer Surplus (PS) in the 1985, 2000 and 2010 reforestation scenario. In both charts, $e \in \{-0.6, -0.3, -0.1\}$ are highlighted with vertical lines.

Figure A.4: Impact of the Demand Elasticity on Thermal Producer Surplus Change

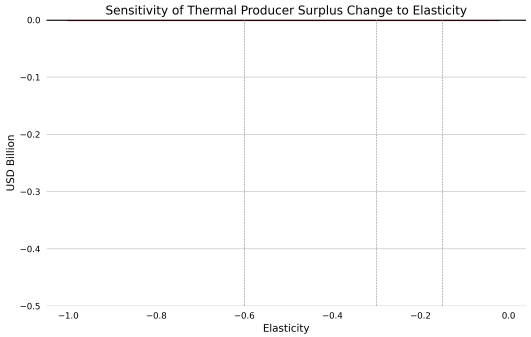
Scenario A: 1985



Scenario B: 2000



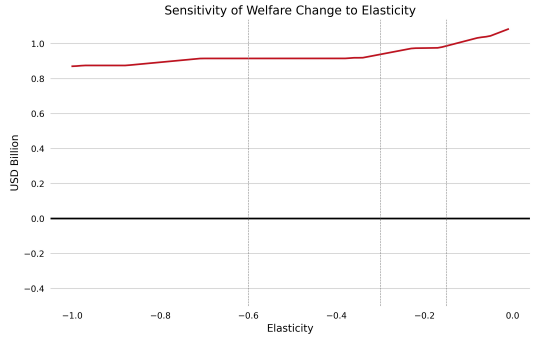
Scenario C: 2010



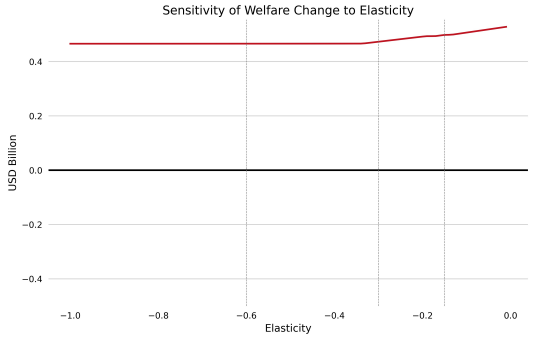
Notes: These charts show the impact of using different demand elasticities on Δ Thermal Producer Surplus in the 1985, 2000 and 2010 reforestation scenario. In both charts, $e \in \{-0.6, -0.3, -0.1\}$ are highlighted with vertical lines.

Figure A.5: Impact of the Demand Elasticity on Total Welfare Change

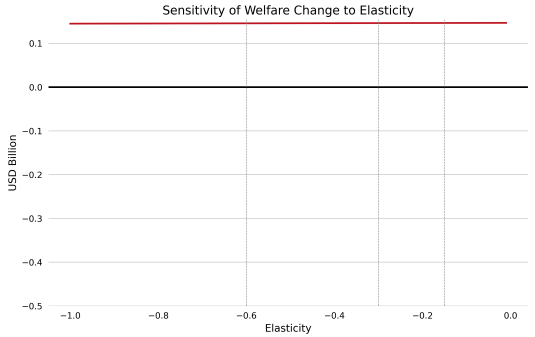
Scenario A: 1985



Scenario B: 2000



Scenario C: 2010



Notes: These charts show the impact of using different demand elasticities on Δ Welfare in the 1985, 2000 and 2010 reforestation scenario. In both charts, $e \in \{-0.6, -0.3, -0.1\}$ are highlighted with vertical lines.

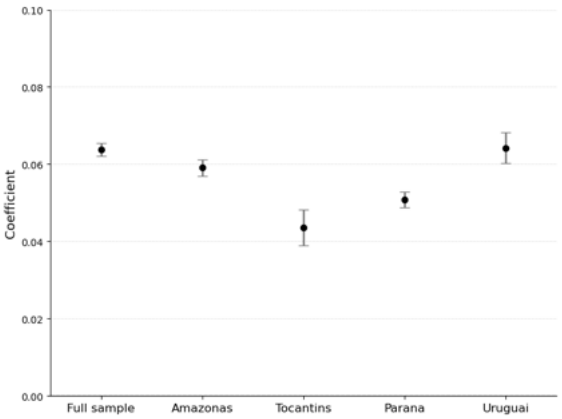
B Additional Figures

This appendix contains some additional figures referenced on the main text. Figure B.1 (a) maps the subsets of basins used on an alternative equation (1). Figure B.1 (b) shows the coefficients of equation (1) estimated for each of the four broader basins—Amazon, Paraná, Tocantins, Uruguai.

Figure B.1: Robustness of the Forest-Rainfall Relationship



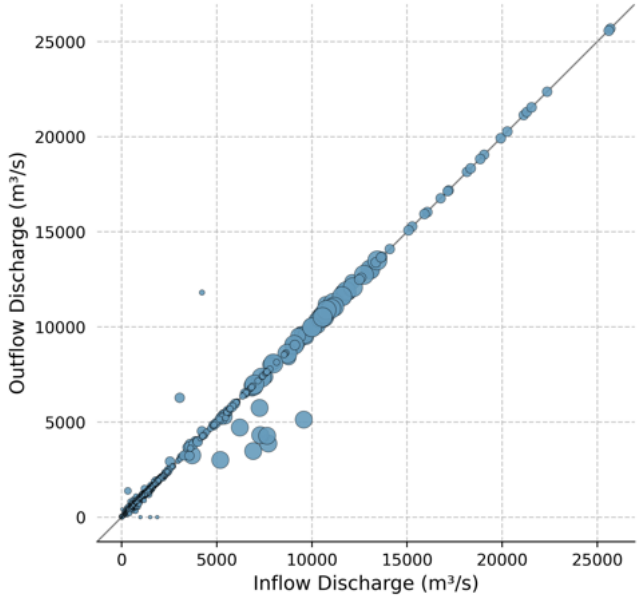
(a) Map of the Alternative Basin Samples



(b) Estimated Coefficients Across the Alternative Basin Samples

Figure B.2 presents the average annual inflow and outflow discharge (in m^3/s) for all hydropower plants in our sample. For the majority of plants, mean inflow approximately equals mean outflow, suggesting that reservoirs do not accumulate substantial water over time. This empirical pattern justifies our simplifying assumption of neglecting storage dynamics in the model. Notably, among the 2,507 observations (one per HP-year) in our sample, only 16 have a significant difference between mean inflow and mean outflow throughout the year.

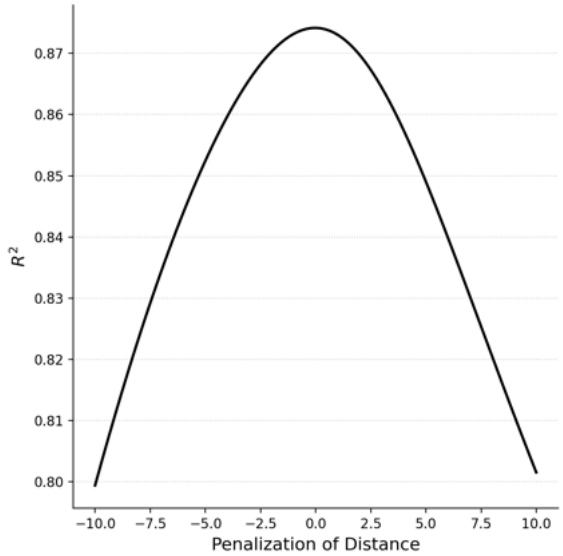
Figure B.2: Average Yearly Inflow and Outflow Discharge (in m^3/s)



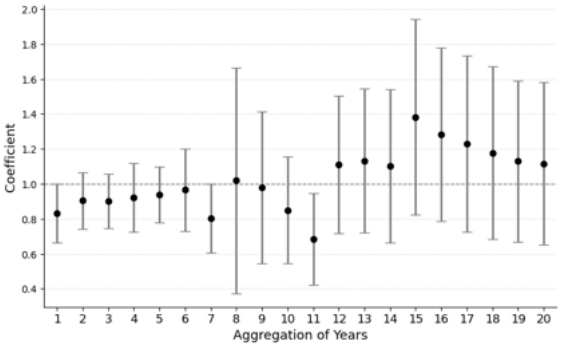
Notes: This figure plots the mean inflow and mean outflow discharge for all hydropower plants in our panel. The 45° line represents the locus where mean inflow equals mean outflow. For the vast majority of plants, observations lie close to this line. Observations are scaled to HPs installed capacity.

Figure B.3 summarizes the validation and robustness results for equation (3). (a) shows how the out-of-sample R^2 responds to different distance penalization factors (see footnote 11). The model achieves its best fit when distance is not penalized. (b) presents the estimated elasticity of river flow with respect to hydropower plant energy output under different temporal aggregations. Across specifications, we cannot reject the null hypothesis that the elasticity equals one, consistent with a one-to-one relationship between discharge and energy output.

Figure B.3: Robustness of the Forest-Rainfall Relationship



(a) Out-of-sample Performance for Different Distance Penalties



(b) Estimated Elasticity of River Flow on Energy

C Computing Granular Forest Contributions to Electricity Market Welfare (Section 7.4)

This appendix details the computation of pixel-level forest contributions to energy market welfare.

Step 1. We compute E_{jmt} by summing, over all downwind pixels $i \in D_{jmt}$, the effect of pixel j's forest on rainfall at i and the effect of rainfall at i on average hydropower generation for plants whose catchment area includes i. This is summarized in equation 11. Two remarks apply. First, rainfall in some pixels may supply more than one power plant as water moves downstream; in those cases, we sum the contribution across all affected plants. Second, E_{jmt} captures the average rather than marginal effect of pixel j's forest on energy output. The marginal effect would require including parameter γ given our log-log specification (equation 3), since the marginal effect of an extra millimeter of upstream rainfall on energy is $\gamma E_{h,0} / \sum_{\ell \in h} r_{\ell,0}$. Because we later scale these contributions, γ is innocuous for the final values.

Step 2. We average E_{jmt} over all months in the sample period,

$$\bar{E}_j = \frac{1}{432} \sum_{m,t} E_{jmt},$$

and scale the resulting distribution so that the total value of forest loss between 1985 and 2020 equals the present value of welfare gain from that scenario: \$21.9 billion. That is, the value of forest in pixel j is

$$v_j = \bar{E}_j \times w, \tag{C.1}$$

where w is the scaling factor satisfying

$$\sum_j v_j \, \Delta p_j = 21.9 \times 10^9, \tag{C.2}$$

and Δp_j is forest loss (in %) in pixel j from 1985 to 2020. From equations (C.1) and (C.2):

$$w = \frac{21.9 \times 10^9}{\sum_j \bar{E}_j \, \Delta p_j}.$$